Transport Pathways of Peroxyacetyl Nitrate in the Upper Troposphere and Lower Stratosphere from different monsoon systems during the Summer Monsoon Season

Suvarna Fadnavis[1], Kirill Semeniuk[2], Martin G. Schultz[3] and Michael Kiefer[4], Anoop Mahajan[1], Luca Pozzoli[5], S. Sonbawane[1]
[1]Indian Institute of Tropical Meteorology, Pune India
[2]Department of Earth and Space Sciences and Engineering, York University, Toronto, Canada
[3]Institute for Energy and Climate Research-Troposphere (IEK-8), Forschungszentrum Jülich, Jülich, Germany
[4]Karlsruhe Institute of Technology, Institute for Meteorology and Climate Research, Karlsruhe, Germany
[5]Eurasia Institute of Earth Sciences, Istanbul Technical University, Turkey

Abstract:

The Asian summer monsoon involves complex transport patterns with large scale redistribution of trace gases in the upper troposphere and lower stratosphere (UTLS). We employ the global chemistry-climate model ECHAM5-HAMMOZ in order to evaluate the transport pathways and the contributions of nitrogen oxide species PAN, NO_x, and HNO_3 from various monsoon regions, to the UTLS over Southern Asia and vice versa. Simulated long term seasonal mean mixing ratios are compared with trace gas retrievals from the Michelson Interferometer for Passive Atmospheric Sounding aboard ENVISAT(MIPAS-E) and aircraft campaigns during the monsoon season (June-September) in order to evaluate the model's ability to reproduce these transport patterns.

The model simulations show that there are three regions which contribute substantial pollution to the South Asian UTLS: the Asian summer monsoon (ASM), the North American Monsoon (NAM) and the West African monsoon (WAM). However, penetration due to ASM convection reaches deeper into the UTLS as compared to NAM and WAM outflow. The

circulation in all three monsoon regions distributes PAN into the tropical latitude belt in the upper troposphere (UT). Remote transport also occurs in the extratropical UT where westerly winds drive North American and European pollutants eastward where they can become part of the ASM convection and lifted into the lower stratosphere. In the lower stratosphere the injected pollutants are transported westward by easterly winds. Sensitivity experiments for simultaneous NO_x and NMVOCs emission change (-10 %) over ASM, NAM, WAM confirm similar transport. Our analysis shows that 10% change in Asian emissions, transport ~5-30 ppt of PAN in the UTLS over Asia, ~1-10 ppt of PAN in the UTLS of Northern subtropics and mid latitudes, ~7-10 ppt of HNO_3 and ~1-2 ppb of ozone in UT over Asia. Comparison of emission change over Asia, North America and Africa shows highest transport of HNO_3 and ozone occurs in the UT over Asia and least over Africa.

The intense convective activity in the monsoon regions is associated with lightning and thereby the formation of additional NO_x. This also affects the distribution of PAN in the UTLS. According to sensitivity simulations with and without lightning, increase in concentrations of PAN (~40 %), HNO_3 (75%), NO_x (70 %) and ozone (30 %) over the regions of convective transport, especially over equatorial Africa and America and comparatively less over the ASM. This indicates that PAN in the UTLS over the ASM region is primarily of anthropogenic origin.

1. Introduction

Deep monsoon convection plays a key role in venting chemical constituents from the boundary layer and their export from source regions (Dickerson et al., 1987). The largest regional monsoon systems are the North American monsoon (NAM), Asian Summer Monsoon (ASM), Western North Pacific monsoon (WNPM), South American monsoon (SAM), West African Monsoon (WAM), and the Australian Monsoon (AUSM) (Chang et al., 2011). Recent observation and modeling studies indicate that the Asian summer monsoon (Park et al., 2004; Li et al., 2005; Randel and Park, 2006; Fu et al., 2006; Park et al., 2007; Xiong et al., 2009; Randel et al., 2010; Fadnavis et al., 2013), the North American Monsoon (Schmitz and Mullen 1996; Collier and Zhang, 2006; Barth et al., 2012) and the West African monsoon (Bouarar et al., 2011) play important roles in the transport of chemical constituents out of the boundary layer into the northern hemisphere in the Upper Troposphere (UT). A Number of studies have documented large amount of pollution transport across tropopause occurs from Asia (Park, 2006; Fu et al., 2006; Park et al., 2007). However transport from other monsoon systems (WAM, NAM) and their contribution to Asia have gotten less attention. Until now there has been no attempt to assess the relative contributions from these source regions and to analyze the transport patterns including possible recirculation within one consistent model framework. Prior model simulations suggest that pollutants transported from the Asian monsoon region can contribute substantially to the budgets of stratospheric ozone, NO_x and water vapour (Randel et al., 2010). Ozone formation in the anticyclone is also enhanced by transport of pollution plumes from the North American monsoon which are rich in volatile organic compounds (VOC) (Li et al., 2005; Zhang et al., 2008; Choi et al., 2009; Barth et al., 2012). The deep monsoon convection over West Africa transports Central African emissions to the upper troposphere and lower

stratosphere (UTLS) leading to large ozone changes in the lower stratosphere (Bouarar et al., 2011). A number of studies have reported transport of chemical constituents into the UTLS due to the Asian monsoon convection, while less attention has been paid to deep convective transport from North/South America and West Africa to the lower stratosphere and to their relative contributions to the UTLS composition over the ASM region.

This study investigates the transport patterns and relative contributions to the Asian monsoon anticyclone of three oxidized nitrogen species, namely peroxyacetyl nitrate (PAN), NO_x (the sum of NO and NO_2), and nitric acid (HNO_3). PAN is a secondary pollutant that marks the transport and conversion of surface NO_x after it is emitted. The focus is placed on PAN as this species has a long lifetime in the UT and can be favorably observed by satellite instruments. At the same time its short chemical lifetime in the lower troposphere results in a much tighter association between the emissions regions of its precursors and transport compared to species such as carbon monoxide (CO). The much longer chemical lifetime of CO in the lower troposphere allows it to reach the UTLS via circuitous pathways that are not accessible to PAN. In contrast, PAN is a tracer that allows for a clearer identification of NO_x pollution transport pathways between the surface and the UTLS. We the perform NO_x and MNVOCs emission sensitivity simulations in order to investigate the relative contributions from Asia, Africa and America to the PAN, HNO_3 and O_3 concentrations in the UTLS.

PAN is formed through oxidation of non methane volatile organic compounds (NMVOCs) in the presence of NO_x (Fischer et al., 2014). It is primarily formed after oxidation of acetaldehyde (CH_3CHO) or after photolysis of acetone (CH_3COCH_3) and methyl glyoxal (CH_3COCHO), all of which are oxidation products of various NMVOCs. The actual formation of PAN proceeds in the reaction of the peroxy acetyl radical (CH_3CO_3) with NO_2. This reaction is reversible and the

thermal decomposition of PAN back to CH_3CO_3 and NO_2 is the main sink of PAN, although in the UTLS PAN photolysis becomes the dominant loss process. Two minor loss processes of PAN are reaction with OH and dry deposition (Talukdar et al., 1995; Fischer et al., 2014). As stated by Fischer et al. (2014) globally, biogenic VOC like isoprene and terpenes contribute most to PAN formation, but in the context of our study it is important to note that the oxidation of many alkanes and alkenes which are emitted from anthropogenic sources lead to PAN formation as well. The major anthropogenic sources of NMVOCs are the emissions from fossil fuel and biofuel combustion and from industrial solvents (Tang et al., 2009). Biomass burning, biogenic and soil emissions also contribute to NMVOC and NO_x production. Anthropogenic sources are dominant in the extra tropical Northern Hemisphere outside the spring season. In spring, when surface PAN peaks, biogenic and anthropogenic NMVOCs species each support about 50% of the PAN burden.

In the UT, lightning can add substantial amounts of NO_x and thus lead to additional PAN production if NMVOC precursors are present, e.g. from convective uplifting from the boundary layer (Tie et al., 2001). The estimated global NO_x production by lightning is ~3 - 5 Tg N/year (Schumann and Huntrieser, 2007; Martin et al., 2007; Murray et al., 2012). Strong lightning activity during ASM, NAM and WAM (Shepon, et al., 2007; Evett et al., 2008; Ranalkar and. Chaudhari, 2009; Barret et al., 2010; Penki and Kamra, 2013) hence contributes to PAN production in the UTLS. The estimated increase in PAN is ~20 - 30 % due to nitrogen enhancement by lightning (Tie et al., 2001).

The thermal decomposition rate of PAN is highly temperature dependent. In the UTLS temperatures are sufficiently low to prevent thermal decomposition of PAN and therefore the

chemical lifetime of PAN in this region is several months (Arnold and Hauck, 1984). The PAN lifetime in our ECHAM5-HAMMOZ simulations varies between 80 and 170 days in the tropical UTLS (figure not included).). Number of studies (Tereszchuk et al., 2013, Glatthor et al., 2007, Sign et al 1987) has reported lifetime of PAN varying form 2 - 4 months. PAN therefore travels over long distances and affects the NO_y partitioning in areas that are far away from the precursor emission regions. Upon descent into warmer regions of the troposphere, PAN releases NO_x which in turn increases ozone and OH production in remote regions (Singh et al., 1986; Singh et al., 1998; Hudman et al., 2004). PAN mixing ratios vary from less than 1 pptv in the remote marine atmosphere (as observed during the NASA GTE PEM-Tropics B campaign in the South Pacific lower marine boundary layer, data available at http://acd.ucar.edu/~emmons/DATACOMP/) to several ppbv in the polluted urban environment and biomass burning plumes (Ridley et al., 1992; Singh et al., 1998). In the UTLS mixing ratios are typically in the range 10-300 pptv (Emmons et al., 2000; Keim et al., 2008).

To our knowledge, this is the first study that analyzes the influence of monsoon outflow from different world regions on the distribution of peroxyacetyl nitrate (PAN) in the UTLS over the Asian monsoon region, and its recirculation in the UTLS. The emission sensitivity simulations were analyzed to understand contribution from ASM, WAM and NAM. We run decadal simulations with the chemistry climate model ECHAM5-HAMMOZ and apply statistical comparisons with satellite and aircraft data, thereby contributing to the objectives of the Chemistry Climate Model Initiative (CCMI, see http://www.igacproject.org/CCMI). The model climatology is evaluated with data from aircraft campaigns and the Michelson Interferometer for Passive Atmospheric Sounding (MIPAS) instrument onboard the ENVIronmental SATellite (ENVISAT) (Refereed as MIPAS-E hereafter). The transport of HNO_3 and NO_x due to monsoon

141 convection from different monsoon regions and the impacts of lightning on the UTLS
142 distributions of the nitrogen oxides are also analyzed and compared to the results obtained for
143 PAN. The paper is organized as follows: Section 2 contains a short description of the data and
144 model including the simulation setup. Comparison of model simulations with observations is
145 given in section 3. In section 4, we discuss the various convective transport pathways of PAN
146 into the UTLS, its redistribution in the stratosphere and its re-circulation across the various
147 monsoon regions, results of emission sensitivity simulations depicting contribution from major
148 monsoon systems. The analysis of percentage changes in lightning produced ozone, HNO_3, PAN
149 and NO_x on total concentrations over the convective zones is presented in section 5. Conclusions
150 are given in section 6.
151

2. Methods

2.1 Satellite measurements

The MIPAS–E instrument onboard the ENVISAT was launched in March 2002 into a polar orbit of 800 km altitude, with an orbital period of about 100 minutes and an orbit repeat cycle of 35 days. MIPAS–E (Fischer and Oelhaf, 1996; Fischer et al., 2008) was a Fourier Transform Spectrometer that provided continual limb emission measurements in the mid infrared over the range 685 – 2410 cm^{-1} (14.6 – 4.15 μm). From January 2005 through the end of the mission in April 2012 MIPAS was operated with a spectral resolution of 0.0875 cm^{-1}, and a stepping of the tangent altitude of 1.5 – 2 km in the UTLS region. As mid infrared sounder MIPAS-E could not provide spectral information from below cloud top.

MIPAS-E monitored several atmospheric trace constituents affecting atmospheric chemistry including PAN, NO_x, and O_3. The details of the general retrieval method and setup, error estimates and use of averaging kernel and visibility flag are documented by Von Clarmann et al. (2009). In this study we analyze the MIPAS-E observed PAN data during the period 2005 – 2012, i.e. the data version V5R_PAN_220/V5R_PAN_221 (different naming 220/221 merely due to technical reasons). The data are available from http://share.lsdf.kit.edu/imk/asf/sat/mipas-export/Data_by_Target/. Details of the MIPAS PAN retrievals, error budget, and vertical resolution are given by Glatthor et al. (2007) and by Wiegele et al. (2012). Table 3 in Wiegele et al. (2012) indicates that for the total error of single profiles of the V5R_PAN_220/221 product the spectral noise and the uncertainty of the instrument pointing are the main contributors. However, since noise is a major contributor a reduction of the total error can be expected for vertical profiles of binned data. For typical bins used in this work the total errors are less than 10 % below 12 km, 30 % at 15 km, 50 % at 19 km and 80 % at 23 km.

The sensitivity of the PAN retrievals can be judged by the averaging kernels. For the V5R_PAN_220/221 product an example of the respective averaging kernel rows is shown in figure S1 for an altitude range of 5 to 25 km at 28 degree N and 85 degree E for cloud free atmospheric conditions. The diamonds indicate the respective nominal altitudes of the retrieval grid. The figure shows that the retrieval results below 8 - 9 km are dominated by information from above the nominal altitude. A similar, albeit less obvious, situation develops for altitudes above 22 - 23 km. There and above the information has an increasing weight from lower than nominal altitudes. This is the reason why the MIPAS PAN data is not considered below 8 km and above 23 km. Another effect clearly visible in the example is that the altitude region which influences the retrieved PAN value at a given altitude is increasing with altitude, i.e. the vertical resolution decreases with altitude. To account for the comparatively low, and altitude dependent, vertical resolution, the model data to be directly compared to MIPAS measurements was convolved with the MIPAS PAN averaging kernel.

The data are contoured and gridded at 4 degree latitude and 8 degree longitude resolution. In the process the data quality specifications as documented at http://share.lsdf.kit.edu/imk/asf/sat/mipas-export/Documentation/ were employed, namely: only data with visibility flag equal 1 and diagonal value of averaging kernel greater than 0.03 were used.

2.2 ECHAM5-HAMMOZ model simulation and experimental setup

The ECHAM5-HAMMOZ aerosol-chemistry-climate model used in the present study comprises of the general circulation model ECHAM5 (Roeckner et al., 2003), the tropospheric chemistry module, MOZ (Horowitz et al., 2003), and the aerosol module, Hamburg Aerosol Model (HAM) (Stier et al., 2005). It includes ozone, NO_x, VOC and aerosol chemistry. The gas

198 phase chemistry scheme is based on the MOZART-2 model (Horowitz et al., 2003), which
199 includes comprehensive O_x-NO_x-hydrocarbons chemistry with 63 tracers and 168 reactions. The
200 $O(^1D)$ quenching reaction rates were updated according to Sander et al. (2003), and isoprene
201 nitrates chemistry according to Fiore et al. (2005). In the model simulations we included
202 emissions of acetone from anthropogenic sources and wild fires (primary sources), while
203 acetaldehyde and methylglyoxal are produced by oxidation of other NMVOCs (secondary
204 sources). In particular, oxidation of primary NMVOCs like ethane (C_2H_6), propane (C_3H_8) and
205 propene (C_3H_6) forms acetaldehyde, while CH_3COCHO is mainly formed from the oxidation
206 products of isoprene and terpenes. Higher acyl peroxy nitrates (MPAN) are included in
207 MOZART-2 chemical scheme, they are also formed through oxidation of NMVOCs, but their
208 production is small compared to PAN. Thermal decomposition, and reaction with OH as well as
209 the absorption cross sections for PAN photolysis are all specified according to Sander et al.
210 (2003).

211 In ECHAM5-HAMMOZ dry deposition follows the scheme of Ganzeveld and Lelieveld
212 (1995). Soluble trace gases such as HNO_3 and SO_2 are also subject to wet deposition. In-cloud
213 and below cloud scavenging follows the scheme described by Stier et al. (2005). PAN is not
214 water soluble, therefore dry and wet deposition are insignificant removal processes.

215 The model is run at a spectral resolution of T42 corresponding to about 2.8 x 2.8 degrees in
216 the horizontal dimension and 31 vertical hybrid σ-p levels from the surface up to 10 hPa. We
217 note that the nominal grid resolution of 2.8 degrees is somewhat misleading, because the spectral
218 truncation of T42 only allows to resolve details on the order of 180/42 = 4.28 degrees. This is the
219 main reason why we compare our model results with the MIPAS PAN retrievals on a 4 x 8

220 degree grid. The details of model parameterizations, emissions and validation are described by
221 Pozzoli et al., (2008a,b, 2011) and Fadnavis et al. (2013).

222 The simulations were performed with varying monthly mean sea surface temperature
223 (SST) and sea ice cover (SIC) data over the period 2000 – 2010 (AMIP) referred as control
224 simulation. The simulations did not aim to exactly reproduce specific meteorological years, and
225 we ran 11-year periods in order to obtain a reasonable statistics. We used the RETRO project
226 data set of the year 2000 available at http://eccad.sedoo.fr/ for the surface CO, NO_x , and
227 hydrocarbon emissions from anthropogenic sources and biomass burning (Schultz et al., 2004;
228 2005; 2007; 2008). Anthropogenic total RETRO emissions of the year 2000 are 476 Tg/year for
229 CO and 90 Tg/year for NO_x, 5 Tg/year of ethane, 3.5 Tg/year of propane and 2.7 Tg/year of
230 propene, which are the main anthropogenic VOC precursors of PAN. Biomass burning RETRO
231 emissions of year 2000 are 357 Tg/year for CO, and 16 Tg/year for NO_x. 2.5 Tg/year for ethane,
232 1.3 Tg/year for propane, 2.7 Tg/year for propene, and 2.7 Tg/year for acetone. CO biomass
233 burning emissions in Southeast Asia account for 7 Gg/month in spring, while up to 15 Gg/month
234 were reported from Carmichael et al. (2003). The anthropogenic and biomass burning emissions
235 of SO_2 (total of 142 Tg/year), BC (7.7 Tg/year) and OC (66.1 Tg/year) are based on the
236 AEROCOM emission inventory (Dentener et al., 2006), also representative of the year 2000. The
237 biogenic NMVOC emissions are calculated on-line with the MEGAN module of Guenther et al.
238 (2006). The simulated global annual mean emission of biogenic NMVOCs between 1995 and
239 2004 is 830 Tg(C)/year, isoprene contributes by 57 %, followed by terpenes (21 %), methanol
240 (12 %), and other NMVOCs such as acetaldehyde (2.5 %) and acetone (2.3 %). Other natural
241 emissions calculated on-line by the model are the Dimethyl Sulfide (DMS) fluxes (Kettle and

242 Andreae, 2000; Nightingale et al., 2000; Pham et al., 1995), sea salt aerosols (Schulz et al., 2004)
243 from the oceans, and mineral dust aerosols (Tegen et al., 2002; Cheng et al., 2008).

244 Our base year for aerosol and trace gas emissions is 2000, and emissions were repeated
245 annually throughout the simulation period. One point to note is that there were substantial
246 emission changes in Asia and Africa (increasing trends) and Europe and North America
247 (decreasing trends) during the study period, which is not captured in our simulations. A
248 consequence of these emission changes for our study would be that we may underestimate the
249 impact from local pollution sources on PAN concentrations in the UTLS over the ASM region in
250 recent years and that we overestimate the contribution from long-range transport of northern
251 hemispheric pollution. We provide an estimate of this error in the discussion of the results.
252 Lightning NO_x emissions are parameterized following Grewe et al. [2001]. They are proportional
253 to the calculated flash frequency with a production rate of 9 kg(N) per flash, and distributed
254 vertically using a C-shaped profile. The calculated flash frequency is resolution-dependent and
255 scaled globally to yield annual global emissions of 3.4 Tg(N) per year. To study the impact of
256 lightning on the distributions of PAN we compare two sets of experiments; each conducted for
257 11 years 2000-2010: (1) the control experiment (CTRL) and (2) the lightning off experiment
258 (light-off).

259 Model simulated PAN, NO_x, HNO_3 and Ozone mixing ratios are evaluated with
260 climatological datasets of airborne campaigns during the monsoon season (June-September). The
261 data were retrieved from http://acd.ucar.edu/~emmons/DATACOMP/CAMPAIGNS/ (see also
262 the paper by Emmons, 2001). The NO_x and ozone volume mixing ratios observed during Cloud
263 Aerosol Interaction and Precipitation Enhancement Experiment (CAIPEEX) (details available in

Kulkarni et al., 2012), September 2010, are evaluated over the Indian region. The details of instruments and measurement techniques are available at http://www.tropmet.res.in/~caipeex/about-data.php. The list of data sets and aircraft campaign used for comparison are presented in Table 1. For the comparison, aircraft observations are averaged over 0 - 2 km, 2 - 6 km and 6 - 8 km and horizontally over the coherent flight regions.

In order to understand the impact of enhanced NO_x and NMVOCs emissions on the distribution of PAN, we conducted a reference and 3 sensitivity simulations for the year 2003 driven by European Centre for Medium-Range Weather Forecasts operational analyses (Integrated Forecast System (IFS) cycle-32r2) meteorological fields (available every 6 h) (Uppala et al., 2005). Model simulations were performed for the year 2003 since there was no significant oceanic/meteorological perturbation event like, e.g., El Niño Southern Oscillation or the Indian Ocean Dipole (http://www.marine.csiro.au/~mcintosh/Research_ENSO_IOD_years.htm). In the sensitivity experiments, NO_x and NMVOCs emissions were reduced by 10% simultaneously over the monsoon regions. The experiments 1 to 3 were performed with reduced emissions over (1) Asia (10S-50N, 60-130E), (2) Africa (30S-30N, 15W-45E), and (3) North America (15N-45N, 120W-75W), refereed as Asia-10%, Africa-10%, North-America-10%.

2.3 Model production of PAN

PAN is a secondary pollutant that has a short lifetime in the lower troposphere. This reduces the number of source points that contribute to PAN concentrations at any location in the UTLS resulting in a clearer identification of source-receptor pathways. Figure 1 shows the distribution of PAN production at 14 km and 16 km. A striking feature is the confinement of PAN production

286 to regions of deep convection. A maximum daily production rate of PAN in the UTLS, in these
287 convective zones, is >24 ppt/day near 14 km and >12 ppt/day near 16 km. Production of PAN
288 from background concentrations of ethane (C_2H_6) and other NMVOCs outside of deep
289 convection regions is distinctly secondary. NMVOCs are subject to the same convective
290 transport as NO_x and PAN formation occurs where both have the highest values. The lifetime of
291 NO_x is short throughout the troposphere which implies that PAN production in the UT will be
292 associated with deep convection. There is also a contribution to PAN production from
293 stratospheric air penetrating into the troposphere (Liang et al., 2011). Tropopause folding is a
294 significant source of exchange between the stratosphere and the troposphere (Gettelman et al.,
295 2011). This is an extratropical process that is only likely to contribute to the PAN formation
296 maxima over North America, Europe and Asia shown in Figure 1(a) via enhanced conversion of
297 ethane. In the model it is unable to obscure the relationship between PAN formation and NO_x
298 pollution source regions.

299 **3. Comparison of model simulations with observations**

300 **3.1 Comparison with aircraft measurements**

301 Figure 2 shows scatter plot between aircraft observations and model simulations at the coherent
302 locations. Both aircraft observations and model simulations are averaged for the monsoon season
303 and altitude ranges. It indicates that model simulated PAN,O_3 and NO_x show good agreement
304 with aircraft measurements, correlation coefficient >0.7 and significance (P-value) varies
305 between 0.00 to 0.3 indicating correlation is significant at 95% confidence level. However
306 simulated HNO_3 between 2 - 6 km and 6 -10 km does not agree well with aircraft observations.

The point to point comparison of (latitude-longitude transects at various altitudes) simulated PAN, NOx, O_3 and HNO_3 with aircraft observations are presented by Fadnavis et al. (2014). These plots show good agreement between model simulations and aircraft observations. Vertical variation of simulated ozone also shows good agreement with ozonesonde measurements over India (see supplementary figure S3 in Fadnavis 2014). Figures sharing the difference between ECHAM5-HAMMOZ and the aircraft observations are provided in the supplement as Figure S2. The model bias varies with species and altitude. In general bias in PAN is -20 ppt to 80 ppt, ozone -2ppb to 40 ppb, HNO_3 -20ppt to 75 ppt. NO_x mixing ratios show good agreement with CAIPEEX measurements over the Indian region. Unfortunately, there were no measurements of PAN or HNO_3 made during CAIPEEX.

3.2 Comparison with MIPAS-E retrievals

In order to study the influence of monsoon circulation on the distribution of PAN in the UTLS region, multi-year averages (2005-2011) of seasonal mean (June-September) PAN retrievals from MIPAS-E are analyzed. Figure 3 (a) presents these data for the altitude range 14 - 16 km, and Figure 3 (b) shows the corresponding ECHAM5-HAMMOZ results for comparison. MIPAS-E observations show maximum PAN mixing ratios (~200 - 230 ppt) over (1) the Asian monsoon anticyclone region (12^O – 40^O N, 20^O - 120^O E), and (2) over parts of North America, the Gulf Stream, (3) southern Atlantic Ocean and west coast of tropical Africa. ECHAM5-HAMMOZ CTRL simulations also show high PAN concentration at these locations, however PAN concentrations are lower than MIPAS-E observations and appear somewhat more localized. MIPAS-E exhibits a PAN maximum originating from African sources over the South Atlantic, whereas the model shows this maximum over the African continent. This may be the outflow of

biomass burning over central and southern Africa during summer monsoon, which might be underestimated in the model. The biomass burning region of Africa during the ASM season is ~30^{O} S - 20^{O} N; 20^{O} W - 30^{O} E (Glanter et al., 2000). The longitude-altitude and latitude-altitude cross-sections of MIPAS-E observed and simulated PAN over the biomass burning region are plotted in figure S3. Model simulation shows that the biomass plume rising from Africa move westward and northward over the Atlantic Ocean and merges with South American plume. From satellite, aircraft observations and model simulations Real et al., (2010), and Barret et al., (2008) reported a plume in the mid and Upper Troposphere (UT) over the southern Atlantic which originates from central African biomass burning fires.

The difference between ECHAM5-HAMMOZ simulation and MIPAS observations plotted in figures S3 (c) and S3 (f). These figures show that the model underestimates biomass burning PAN by 20 - 60 ppt. These differences may also be related to issues in the vertical transport of PAN, or to a possible underestimate of the emission sources of NMVOCs. Uncertainties in the rate coefficients and absorption cross sections of PAN may also play a role. Furthermore, anthropogenic NO_x emissions are mostly underestimated in the emission inventories (Miyazaki et al., 2012). As discussed in Fadnavis et al. (2014), UTLS PAN over the ASM is sensitive to NO_x emission changes in India or China. In their study, also performed with ECHAM5-HAMMOZ, a 73 % NO_x emission change in India lead to a PAN increase of 10 - 18 %, while a 73 % NO_x emission change in China changed PAN over the ASM by 18 - 30 %. The cross-section plots of (see figure S4) differences in MIPAS-E PAN with model simulated PAN indicate that in the UTLS (8 - 23 km), MIPAS-E PAN is higher than model simulated PAN by ~20 - 60 ppt (except above 20 km). It is lower by 20 - 40 ppt over eastern part of anticyclone (Southern India and South east Asia) and also over Indonesia and northern Australia. In general,

in the ASM region during the monsoon season MIPAS-E PAN is higher than model by 30 - 60 ppt between 8 - 16 km and the difference between MIPAS-E and model PAN vary between +40 ppt to -40 ppt between 17 and 23 km.

4. Transport of PAN during monsoon season

4.1 Transport from Northern tropical land mass

Figure 3(a) shows high concentrations of MIPAS-E PAN at 14-16 km over Asia, North America and tropical Africa. ECHAM5-HAMMOZ simulations (figure 3b) also show similar distribution. This may be due to transport from boundary layer into the UTLS by the monsoon convection from respective regions. ECHAM5-HAMMOZ simulated OLR and 850hpa winds averaged for the monsoon season are shown in Figure S5(a). They indicate the extent of deep convection near the surface. NECP reanalysis OLR and 850 hPa winds averaged for monsoon season (2000-2010) are plotted in figure S5 (b) for comparison. These figures indicate that the model could reproduce deep convection and large scale circulation at the surface. Cross-section of distribution of simulated Cloud Droplet Number Concentration (CDNC) and ice crystal number concentration (ICNC) over Asia, North America and tropical Africa confirms strong convective transport from these regions (figure S5 (c)-(e)). It should be noted that vertical velocities in a large scale model also indicate rapid uplift in deep convective regions. From Satellite observations and model simulations Park et al., (2009) reported transport of fraction of boundary layer Carbon monoxide (CO) into the UTLS by the Asian monsoon convection.

To illustrate vertical transport, longitude-altitude cross sections of PAN mixing ratios averaged over the region 0^{O} - 30^{O} N and for June-September as obtained from MIPAS-E and

ECHAM5-HAMMOZ are shown in Figures 4(a) and (b) respectively. Both MIPAS-E observations and ECHAM5-HAMMOZ simulations show elevated levels of PAN (200 - 250 ppt) near 80^{O} E - 100^{O} E (ASM), 30^{O} W - 30^{O} E (WAM) and 80^{O} W - 100^{O} W (NAM) region. The simulated PAN distribution along with winds plotted in Figure 4(b) show cross tropopause transport from these regions. It reveals that transport of boundary layer PAN to UTLS mainly occurs from strong convective regions, i.e. Bay of Bengal (~80^{O} E - 90^{O} E), South China Sea (~100^{O} E - 120^{O} E), western Atlantic Ocean (Gulf Stream region) and Gulf of Mexico (80^{O} W - 100^{O} W). MIPAS-E observations and model simulations show that the transport due to ASM is strongest and reaches deepest into the lower stratosphere. This is due to the more intense deep convection activity over the ASM region compared to the NAM region. Figure 4(c) presents the differences between MIPAS and model simulated PAN. It appears that the model PAN is overestimated over the ASM (20 - 30 ppt) and underestimated over the NAM (50 - 70 ppt) and WAM (20 - 50 ppt) regions between 8km and 18km. However, the overestimation in the UT in the ASM is difficult to explain on physical grounds and is more likely to be a MIPAS-E sampling issue as discussed later.

4.2 Transport from southern tropical land mass

In order to understand transport of PAN due to southern WAM, SAM and AUSM, we show longitude-pressure sections of MIPAS-E observations and model simulated PAN concentrations averaged over 0^{O} - 25^{O} S in Figure 4(d)-(e) respectively. The model has plumes near 20^{O} E, 100^{O} E and 80^{O} W. These three regions of convective transport are (1) tropical southern Africa 10 -40^{O} E, referred to as South Africa, (2) Indonesia and northern parts of Australia ~100^{O} -110^{O} E and (3) South America ~70^{O} - 80^{O} W. Outflow from Indonesia and from northern parts of Australia

(~100^{O} E) penetrates deep into the UTLS. Tropical Rainfall Measuring Mission (TRMM) satellite observations show high frequency of intense overshooting convection over these areas (during the monsoon season) with highest density in the belt 0^{O} - 10^{O} S over the Caribbean, Amazon, Congo and Southern Maritime Continent (Liu and Zipser, 2005). The analyses of vertical winds show strong transport from10^{O} - 40^{O} E, 100^{O} - 110^{O} E, 70^{O} - 80^{O} W (in the belt 0^{O} - 10^{O} S) (figure not shown). The amount of high level cloud fraction is also high over these regions. Distribution of CDNC and ICNC show deep convection over these regions (Figure not shown). The model simulations show high PAN concentrations reaching the UTLS. Thus transport due to deep convection is reasonably well captured by the model. However, the MIPAS-E retrievals only show a plume rising over South Africa and no enhancement over the AUSM (Indonesia-Australia) and SAM regions. Figure 4(e) shows that the plumes from the three outflow regions are mixed in the UT (8 - 14 km) by the prevailing westerly winds. The reasons for a single plume seen in MIPAS-E may be that lower concentrations of PAN reach these altitudes (above 8 km) from SAM and AUSM and mix with the plume over South Africa. There are indications of elevated PAN concentrations at the lower boundary in Figure 4 (d). Simulations show lower PAN mixing ratios over the longitudes of SAM and AUSM (see figure 4(e)). The differences between MIPAS observations and simulations (figure 4(f)) show that model PAN is overestimated in the AUSM (10-30ppt) and is underestimated over the southern WAM (20 - 70 ppt) and SAM (20 - 50 ppt) between 10 km and 18km. It is likely that the three plume structure in the UT seen in model is being obscured in the observations due to sampling issues since periods of deep convection reaching significantly above 8 km are associated with significant cloud cover.

Figure 4 shows that simulated transport of PAN due to ASM, NAM and WAM convection are stronger and penetrate deeper into the UT compared to SAM and AUSM. This is consistent with the distribution of deep convection noted by Gettelman et al. (2002). In general, the PAN amounts in the UTLS in the model are less than those observed by MIPAS-E. This may be due to an underestimate of the chemical PAN source from VOC precursors or too little vertical transport or a combination of both. Earlier model studies with ECHAM also exhibited too low concentrations of CO in the upper tropospheric outflow (M. Schultz, unpublished data from the NASA Global Tropospheric Experiment TRACE-P mission).

4.3 Transport from Asian Summer Monsoon region

The ASM anticyclone extends from 60^{O}E to 120^{O}E and 10^{O}N to 40^{O}N (see figure 3 (b)). Latitude-altitude cross sections over the ASM anticyclone (60^{O} E - 120^{O} E) of MIPAS-E observed PAN (plotted in the altitude range 8 - 20 km) and ECHAM5-HAMMOZ CTRL simulations are shown in Figures 5(a) and (b), respectively. ECHAM5-HAMMOZ simulations are similar to MIPAS-E retrievals of PAN. There is indication of plume ascent into the lower stratosphere. The ECHAM5-HAMMOZ simulations also show transport of subtropical boundary layer PAN into the UTLS due to deep convection. This is not visible in the MIPAS-E data because of the lack of data below 8 km. Figure 5 (b) shows that there is transport from 40^{O} - 50^{O} N reaching up to 10 km (~200 hPa). Park et al. (2004, 2007, 2009) and Randel and Park (2006) noted that trace species are introduced into the monsoon anticyclone at its eastern end around 200 hPa. The uplift over south-east Asia and the base of the Himalayas in India pumps tracers into the upper tropical troposphere where they get horizontally redistributed by the anticyclonic circulation and form the region of high PAN values between 40^{O} N and high latitudes. Figure

10(c) shows that the mid-latitude maximum seen in Figure 5(c) is due to pollution transport from Europe. The Chinese emissions are feeding into this large plume over Russia and are transported partly and diluted over the extratropical Pacific Ocean. The latitude-altitude section of differences between MIPAS and simulated PAN indicates that ASM plume is underestimated in the model (see figure 5 (c)). It is interesting to compare figure 4(c) (longitude –altitude section) and figure 5(c) (latitude-altitude section). The reason for underestimation of the ASM plume in the latitude-altitude section may be due to a lower contribution from the eastern part of anticyclone in the model. Figure S4 shows model PAN is underestimated over Southern India and South East Asia in the UT and overestimated in the lower stratosphere.

In order to understand the impact of transport from ASM region on the rest of the world, we analyze difference between reference and Asia-10% simulations (reference –Asia-10%). The latitude altitude and longitude altitude cross sections over the ASM region (Figures 5 (d) and 5(e)) show transport of ~5-20 ppt of PAN into the lower stratosphere. The horizontal cross sections at 14 km to 21 km (figures 5 (f) – 5(i)) show that Asian PAN is transported to northern Atlantic by subtropical westerly winds. These figures show that 10% change in Asian emissions (NO_x and NMVOCs), transport ~5-30 ppt of PAN in the UTLS over Asia and 1-7 ppt of PAN in the UTLS of Northern subtropics and mid latitudes.

4.4 Transport from North American monsoon region

Figures 6(a) and (b) exhibit latitude-altitude sections of PAN from MIPAS-E retrievals and ECHAM5-HAMMOZ simulations (seasonal mean for July-September) over the North American

463 monsoon region between 70^{O} W - 120^{O} W. MIPAS-E observations and the model indicate
464 transport of PAN into the UTLS. The distribution of ECHAM5-HAMMOZ simulated PAN from
465 the boundary layer to UTLS shows the source region is at around 40^{O} N. There is convective
466 uplift of PAN over the northern Gulf of Mexico region and over the Gulf Stream. High amount
467 of pollutants are emitted from north east America from a number of power plants are located in
468 Atlanta, Washington, Chicago, Boston, Jacksonville (CEC report, 2011). The tropospheric NO_2
469 columns retrieved from the SCIAMACHY and OMI satellite instrument shows high amount of
470 anthropogenic NO_2 emissions over this region (Lamsal et al., 2011, Miyazaki et al., 2012). The
471 model simulations show high amount of PAN concentrations over this region (see figures 10(a)-
472 (d)). The monsoon convection lifts these pollutants to the UT. The outflow of these pollutants is
473 over the Atlantic (see figures 3 (a)). TRMM precipitation radar observations show significant
474 overshooting convective activity over this region during the monsoon season (Liu and Zipser,
475 2005). The vertical distribution of differences in MIPAS and simulated PAN shows that PAN is
476 underestimated (see figure 6(c)) over North and South America (10-60 ppt) between 10-18km,
477 however it is over estimated between 8-10km in the region near 30^{O}N . As discussed above this
478 may be associated with European emissions and transport.

479 Figures 6 (d) - 6 (e) show impact of North American emission (reference – North-Amrica-10%)
480 on the transport of PAN. It shows cross tropopause transport of PAN by North American
481 monsoon convection. The amount of PAN transported (~1-5 ppt) into the lower stratosphere is
482 less than the ASM (~10-20 ppt). The latitude-longitude distribution of PAN (figures 6 (f) – 6(i))
483 shows that the upper tropospheric westerly winds transport ~1-10 ppt of PAN to Atlantic, Europe
484 and North China.

485 ### 4.5 Transport from West African region

486 Figures 7 (a) - (b) show vertical distributions of PAN over the African region (averaged
487 over 0^{O} - 45^{O} E). MIPAS-E observations and model simulations indicate a plume that crosses the
488 tropopause and enters the lower stratosphere. The model surface fields (see Figure 7(b)) show
489 that this plume arises from latitudes 5-20^{O}S over Africa and that it moves equatorward. It
490 subsequently merges with the ASM plume. A prominent tongue of high PAN values between
491 30^{O} and 60^{O} N is captured in model simulations. This feature appears to be related to emissions
492 from Europe being transported towards the equator in the upper subtropical troposphere.
493 However, in the model, emissions from Europe are transported poleward instead of equatorward
494 (Figure 7(b)). There is a region of strong descent in the model between 30^{O} N and 40^{O} N (see
495 Figure 7(b)) which deforms the PAN isopleths around 12 km around 30^{O} N. This feature is not
496 seen in the MIPAS-E retrievals and indicates a disagreement of the model with the transport
497 pattern of the atmosphere in this region. The transport of PAN in the 10^{O} - 20^{O} S latitude band
498 over the Congo, Angola, Tanzania regions of southern and tropical Africa is not pronounced in
499 the model compared to MIPAS-E observations. This behavior indicates that deep tropical
500 convection is underestimated in the model in this latitude band. The vertical distribution of
501 differences in MIPAS and simulated PAN (figure 7(c) shows that simulated PAN is
502 underestimated over these regions (5^{O} - 20^{O} S and 20^{O} - 40^{O} N) between 10 km and 18 km. The
503 reason may be related to underestimation of deep tropical convection in the model in this latitude
504 band. Simulated PAN is overestimated between 8km and 12km near equator.

505 The reference - Africa-10% simulations (figures 7(d)-7(e)) shows that African PAN is
506 transported up to the tropopause. The cross sections over North and South Africa show

507 penetration of North African plume into the lower stratosphere (~19km). However, PAN
508 transport into the lower stratosphere (~0.2-0.6 ppt) is comparatively less than Asia or North
509 America. Figures 7 (g) - 7(j) show transport of ~5-50 ppt of PAN in the UT (6-12km) of tropical
510 Africa. There is transport from equatorial Africa to Atlantic and Mexico between 6-8km (figures
511 7 (g) – 7 (h)) which is then transported to North China by upper tropospheric (12km) westerly
512 winds (see figures 7 (j)).

513 The model simulated latitude-altitude, longitude-altitude cross sections of NO_x, and
514 HNO_3 over the ASM (10^O N - 40^O N, 60^O - 120^O E), NAM (10^O N - 40^O N, 70^O W - 120^O W) and
515 WAM (0^O - 25^O S, 0^O - 45^O E) are shown in Figures 8 (a) – 8(j), respectively. Figures 8 (a)- 8(e)
516 show transport features of NO_x. These are similar to those seen in the distribution of PAN, but
517 with sharper signatures due to the shorter lifetime of NO_x. This shows that monsoon convection
518 lifts boundary layer pollutants including NOy species to the UTLS. The distribution of HNO_3
519 (see Figures 8 (f) - 8(j)) shows a complex pattern. Comparing Figure 4(b), the region around
520 100^O E with intense convective uplift corresponds to HNO_3 depletion from the surface to above
521 10 km. In fact, the upper tropospheric region of the ASM anticyclone exhibits much lower values
522 of HNO_3 compared to all the other longitudes in the 10^O - 40^O N band (Figure 8(h)). This
523 suggests that in the model the convective transport in the ASM region is associated with efficient
524 removal by wet scavenging. In contrast, the North American monsoon region has HNO_3
525 ascending to the UT with significantly less loss. This is likely due to the fact that convection
526 involved in vertical transport during the NAM is not as intense and not as deep as in the case of
527 the ASM and there are differences in wet scavenging. Figure 8(g) shows that the plume rising
528 from South America moves towards the equator but does not have the extension into the UT as
529 the North American plume. These are June-September averages and the ITCZ is on the northern

hemisphere side during this period. Thus, weaker convective transport is to be expected on the southern hemisphere side of the equator during this period. Figure 8 (i) shows significant transport of African emissions around ~0^{O} - 15^{O} S and a plume rising from Europe (~35^{O} N - 60^{O} N) as well.

Figures 9 (a) –9 (f) show vertical distribution of HNO_3 and O_3, over Asia, North America and Africa as obtained from difference between reference and Asia-10%, North-America-10% and Africa-10% simulations. It is evident that transport of HNO_3 for Asia-10% simulation is deeper in the UT (~16km) than North-America-10% and Africa-10% simulations. It can be seen that Asia-10%, North-America-10% and Africa-10% simulations transport ~7-10 ppt, ~5-7 ppt and ~3-5 ppt of HNO_3 in the UT of their respective regions.

In the UT, between 6km and 10km, Asia-10% simulation shows transport of ~10-15 ppt of HNO_3 over Western Pacific and ~3-10 ppt over tropical America by the subtropical westerly winds (figure not included). North-America-10% simulation shows transport of ~5-7 ppt of HNO_3 over Atlantic, North Africa, Saudi Arabia and North China by the subtropical westerly winds and ~3-5 ppt of HNO_3 over equatorial pacific, Indonesia, China and India by the tropical easterly winds. Africa-10% simulation shows transport of ~3-5 ppt HNO_3 from North Africa to North America, equatorial pacific, also there is transport of ~4 ppt of HNO_3 from South Africa to Atlantic, South America, Indonesia, China and India by the tropical easterly winds (figure not included).

North-America-10% simulation shows transport of boundary layer ozone extending up to the tropopause, which are higher than for the Asia-10% and Africa-10% simulations (figures 9 (d) – 9 (f)). Asia-10%, North-America-10% and Africa-10% simulations show transport ~1-2 ppb, ~0.8-1.5 ppb and ~0.4-0.6 ppb of ozone in the UT of their respective regions.

In the UT, between 6km and 10 km, Asia-10% simulation shows transport of ozone ~1.5 ppb to Western Pacific and 0.8 ppb to Mexico and United States by the subtropical westerly winds (figure not included). North-America-10% simulation shows transport of 0.4-1.5 ppb of O_3 to equatorial Pacific extending up to Indonesia by the tropical easterly winds. There is some outflow (~0.6ppb) over Atlantic by the subtropical westerly winds as well (figure not included). Africa-10% simulation shows transport of ~0.4-0.8 ppb of ozone to equatorial Atlantic and Mexico (figure not included).

It can be seen that similar emission change over Asia, North America and Africa causes highest change in HNO_3 and Ozone in the UT over Asia and least over Africa. In the UT, between 6km and 10 km, transport of HNO_3 by Asia-10% (~3-10 ppt of HNO_3 to tropical America) is higher than North-America-10% (~3-7 ppt of HNO_3 to China and India) and Africa-10% (~3-5 ppt of HNO_3 to tropical America, China and India). Similarly ozone transport is higher for Asia-10% than North-America-10% and Africa-10% simulations.

4.6 Horizontal transport

PAN concentrations from MIPAS-E and ECHAM5-HAMMOZ at different altitudes are analyzed to understand horizontal transport. Figure 10(a) shows the distribution of PAN from ECHAM5-HAMMOZ simulations near the surface (2 km). Sources of PAN are apparent over South America, southern Africa, North America, Europe, Russia and northern China/Mongolia. The PAN distribution at 4 km (see Figure 10(b)) shows high concentrations above these regions indicating vertical transport. Figures 10(c) and 10 (d) show the distribution at 6 km and 8 km. The upper level anticyclonic circulation between 10^O N and 30^O S over the Atlantic transports PAN from central Africa towards America and from Brazil towards southern Africa. The Large

Scale Biosphere-Atmosphere Regional Experiment in Amazonia (LBA-CLAIRE-98) campaign observations (Andreae et al., 2001) and African Monsoon Multidisciplinary Analysis (AMMA) project (Real et al., 2010) show that the biomass burning plume originating from Brazil is lifted to altitudes around 10 km. This plume is entrained into deep convection over the northern Amazon, transported out over the Atlantic and then returned to South America by the circulation around a large upper-level anticyclone. This transport is well captured by the model.

North American pollution is also being transported by the westerly winds over Eurasia, forming an organized belt. This transport pattern persists up to 12 km (Figure 10 (e) and 10(g)). MIPAS-E observations at 12 km also show this transport pattern. The source region for the PAN from southern Africa is the region of active biomass burning. Since this region is tropical, the outflow is over the Atlantic due to the prevailing easterly winds. ECHAM5-HAMMOZ simulations show similar transport (see Figures 10(e)). But there are differences; in particular the transport over tropical Africa does not get displaced over the Atlantic Ocean. As noted above, there are significant transport differences between the model and observations in this longitude band. Another difference is that PAN is not transported westward over Central America and towards the Pacific Ocean.

Figures 10(f)-10(h) show the distribution of PAN from ECHAM5-HAMMOZ simulations and MIPAS-E retrievals , in the lower stratosphere (18 km). In both data sets PAN is transported westwards from ASM, NAM and WAM by prevailing easterly winds and maximizes in the region of the ASM anticyclone.

As can be seen from the above discussions, the ASM, NAM, and WAM outflow and convection over the Gulf Stream play an important role in the transport of boundary layer pollution into the UTLS. Previous studies (e.g. Fadnavis et al., 2013) indicated that over the

Asian monsoon region, transport into the lower stratosphere occurs and there is significant vertical transport over the southern slopes of the Himalayas (Fu et al., 2006, Fadnavis et al., 2013) and also over the region spanned by the Bay of Bengal and the South China Sea (Park et al., 2009). Pollutant transport due to North American convection and tropical African outflow does not penetrate as deep into the stratosphere as the ASM. However there is clear indication that in the UT, middle latitude westerly winds connect the North American pollution to the ASM.

Figures 3-7 and figure 10 show that in the UT, westerly winds drive North American and European pollutants eastward to at least partly merge with the ASM plume. Strong ASM convection transports these remote and regional pollutants into the stratosphere. The Caribbean is a secondary source of pollutant transport into the stratosphere. In the stratosphere the injected pollutants are transported westward by easterly winds and into the southern subtropics by the Brewer-Dobson circulation.

5.0 Impact of Lightning on tropospheric PAN, NO_x, HNO_3 and ozone

In the ASM region and during the monsoon season the NO_x released from intense lightning activity enhances the formation of PAN, HNO_3 and ozone in the middle and upper troposphere which is already relatively strong due to the intense solar radiation along with high background concentrations of NO_x, HO_x and NMVOCs (Tie et al., 2001). PAN, HNO_3 and O_3 produced from lightning may get transported in the lower stratosphere by deep monsoon convection and contribute to anthropogenic emission transport of these species. In order to understand contribution of lightning and the dominating lightning production regions, we analyze difference

between control and light-off experiments. Figure 11(a)-(d) shows the percentage changes in ozone, HNO_3, PAN and NO_x due to lightning as zonally averaged spatial distribution of seasonal mean (June-September) mixing ratios. The analysis indicates that the impact of lightning on these species is largest in the tropical UT between 40^O N -40^O S and between 8 km and 14 km. In the tropical mid troposphere lightning produced maximum ozone is ~15 – 25 % (12 - 24 ppb) , HNO_3 ~ 40 – 60 % (50 -90 ppt) ~ PAN ~15 – 25 % (70 - 140 ppt) and NO_x ~20 – 40 % (10 - 35 ppt) while in the UT ozone is ~20 -30 % (20 - 28 ppb), HNO_3 ~60 - 75% (80 - 110 ppt), PAN ~28 – 35 % (120 - 170 ppt), and NO_x ~50 – 75 % (20 - 65 ppt). Our results are consistent with model simulations by Tie et al., (2001) and Labrador et al. (2005). The spatial distributions of NO_x, ozone, PAN and HNO_3 produced from lightning (see figures 12 (e) – (h)) indicate that in the UT (12 km) increases in O_3 ~20 - 25 % (11 - 17 ppbv), HNO_3 ~40 – 70 %, PAN ~25 – 35 % and NO_x ~55 - 75 %, over North America are in agreement with previous studies (e.g Labrador et al., 2005; Hudman et al. 2007; Zhao et al., 2009; Cooper et al., 2009), over equatorial Africa (PAN 30 - 45 %, HNO_3 ~70 - 80 %, O_3 ~ 25 %, NO_x~70 %) agrees well with Barret et al., 2010; Bouarar et al., 2011 and over the ASM region (PAN ~ 25 %, HNO_3 ~65 -70 %, O_3 ~20 %, NO_x ~ 60 - 70 %) agrees with Tie et al., (2001). These regions coincide with regions of convective vertical transport of PAN (as seen in figures 4 and 5). Lightning produced PAN will be lifted into the lower stratosphere by the monsoon convection along with anthropogenic emissions and will redistribute in the tropical lower stratosphere. Latitude-longitude cross sections of lightning induced PAN, NO_x, ozone and HNO_3 formation at altitudes between 8 - 14 km show that the production of PAN, NO_x, ozone and HNO_3 is less over the ASM region than over the equatorial Americas and Africa (also seen in figure 11). The high amounts of PAN over the ASM are therefore primarily due to anthropogenic emission transport into the UTLS from the source

645 regions in Southern and Eastern Asia. As discussed in Fadnavis et al., 2014, NO_x emissions are
646 estimated to have changed by 38 % in India and 76 % in China, respectively during 2002 - 2011
647 period. From sensitivity simulations they deduced corresponding changes in upper tropopsheric
648 PAN are > 40 %, O_3 by > 25 % and HNO_3 by > 70 % over the Asian monsoon region. These
649 effects are larger than the impact of lightning NO_x emissions over this region (figure 11 (e)-(h)).
650

6. Conclusions

In this study statistical analysis of simulated and satellite-retrieved mixing ratios of PAN, NO_x, and HNO_3 is presented in order to determine the transport patterns of pollution into the Asian monsoon region and the impact of pollution flowing out of the ASM into other regions of the global atmosphere. The analysis focused on the upper troposphere and lower stratosphere and covered the period 2002 - 2011. NO_x and NMVOCs emission perturbation simulations were performed over ASM, NAM and WAM to understand transport pathways and relative contribution impact on the UTLS. As discussed in Fadnavis et al. (2014), NO_x emissions are estimated to have changed by 38 % in India and 76 % in China, respectively during this period. From sensitivity simulations they deduced corresponding changes in upper tropospheric PAN > 40 %, O_3 by > 2 5% and HNO_3 by > 70 % over the ASM region. These effects are larger than the impact of lightning NO_x emissions over this region discussed in section 3 of this study.

Interestingly, the ECHAM5-HAMMOZ reference simulation reveals that in the UT, westerly winds drive North American and northward propagating South African pollutants eastward where they mix with the ASM plume. Deep convection and strong diabatic upwelling in the ASM, convectively transports a part of these plumes into the lower stratosphere. The Caribbean region is another source of pollution transport into the stratosphere. Some cross tropopause transport occurs due to convection over North America and Southern Africa as well. Some cross tropopause transport occurs due to convection over North America and Southern Africa as well. In the lower stratosphere the injected pollutants from ASM, WAM and NAM are transported westward by easterly winds and into the southern hemisphere subtropics by the Brewer-Dobson circulation. The emission sensitivity simulations Asia-10%, North-America-

673 10% and Africa 10% confirm these transport pathways. In the southern hemisphere, plumes
674 rising from convective zones of South Africa, South America and Indonesia-Australia are
675 evident in the model simulations, but are not seen in the MIPAS retrievals. PAN concentrations
676 are higher in the plume rising from South Africa than SAM and AUSM. In the UT, they merge
677 by the prevailing westerly winds. MIPAS-E observations in the UTLS show a single plume over
678 South Africa and no enhancement over SAM or AUSM. The reasons for the single plume seen in
679 MIPAS-E may be that although there is uplifting by each of the three monsoon systems lower
680 concentrations of PAN reach these altitudes (above 8 km) from SAM and AUSM until they
681 merge with South African plume. It is also possible that the three plume structure in the UT seen
682 in the model is being obscured in the observations due to sampling issues. Convective cloud
683 cover is strongly associated with deep convection in the ASM region. The MIPAS-E data has a
684 PAN minimum in the UT right in the longitude band of the deep convection over the southern
685 flanks of the Himalayas (Figure 4(a)). This feature is unphysical and clearly identifies a
686 sampling bias. However, the model is also not fully reproducing the latitudinal structure of the
687 PAN in the ASM region UTLS which indicates that there are differences in both the distribution
688 of convection and the large scale circulation.

689 The horizontal transport of PAN analyzed from ECHAM5–HAMMOZ simulations show
690 that the PAN from southern Africa and Brazil is transported towards America by the circulation
691 around a large upper-level anticyclone and then lifted to the UTLS in the NAM region. It is also
692 evident in the Africa-10% simulation.

693 The vertical distribution of simulated HNO_3 over the monsoon regimes shows low
694 concentrations above 10 km at the foothills of the Himalayas. In contrast, the results show strong

uplifting of HNO_3 into the UT with NAM convection. This may be due to the fact that NAM convection is not as intense as the ASM and there may be more wet removal of nitrogen oxides in the ASM convection. The model simulations indicate a higher efficiency of NO_x conversion to HNO_3 over the Indian region compared to NAM.

The change in emission (-10% , NO_X and NMVOCs simultaneously) over each of ASM, WAM and NAM regions show that Asia-10% transport ~5-30 ppt of PAN in the UTLS over Asia and ~1-10 ppt in the UTLS Northern subtropics and mid latitude. North-America-10% simulation shows transport of ~1-5 ppt of PAN over Atlantic, Europe and North China (between 12-14km) and 0.4-3ppt over Asia (near 16km). Africa-10% simulation shows transport from equatorial Africa to Atlantic and North America between 6 – 8 km, which is then transported to Asia by upper tropospheric westerly winds (near 12km).

Transport of HNO_3 is deeper in the UT (~16km) in Asia-10% simulation than North-America-10% and Africa-10% simulations. Asia-10%, North-America-10%, Africa-10% simulations show transport of ozone ~1-2 ppt, 0.8-1.5 ppt and 0.4-0.6 ppt in the UT over respective regions.

In the UT between 6km and 10km, transport of HNO_3 by Asia-10% (~3-10 ppt of HNO_3 to tropical America) is higher than North-America-10% (transport of 3-7 ppt of HNO_3 to China and India) and Africa-10% (~3-5 ppt of HNO_3 to tropical America, China and India) simulations. Similarly transport of ozone is higher for Asia-10% than North-America-10% and Africa-10% simulations. Comparison of emission change over Asia, North America and Africa shows highest transport of HNO_3 and ozone in the UT over Asia and least over Africa.

Lightning production of NO_x may enhance PAN concentrations in the UT and affect its transport into the lower stratosphere. The percentage change in lightning produced ozone, HNO_3, PAN and NO_x has been evaluated with a sensitivity simulation. In the UT, lightning causes significant increases in these species over equatorial America, equatorial Africa and the ASM region. These regions coincide with intense convective zones with significant vertical transport. Lighting production is higher over equatorial Africa and America compared to the ASM. However, the vertical distribution shows that higher amounts of PAN are transported into the UT in the ASM region. This indicates that the dominant contribution to PAN over the ASM is from anthropogenic emissions. This is consistent with the fact that anthropogenic emissions in the ASM region are higher than in the NAM and WAM (Lamsal et al., 2011, Miyazak et al., 2012).

Acknowledgements: The authors thank the MIPAS-E teams for providing data and the High Power Computing Centre (HPC) in IITM, Pune, India, for providing computer resources. Authors are also thankful to anonymous reviewers for their valuable suggestions.

References

Andreae, M. O., Artaxo, P., Fischer, H., Freitas, S. R., Grégoire, J.-M., Hansel, A., Hoor, P., Kormann, R., Krejci, R., Lange, L., Lelieveld, J., Lindinger, W., Longo, K., Peters, W., de Reus, M., Scheeren, B., Silva Dias, M. A. F., Ström, J., Velthoven, P. F. J. van and William, J.: Transport of biomass burning smoke to the upper troposphere by deep convection in the equatorial region, Geophy.,Res. Lett., 28, 951-958, 2001.

Arnold F. & Hauck G., Lower stratosphere trace gas detection using aircraft-borne active chemical ionization mass spectrometry, Nature, 315, 307-309,| doi:10.1038/315307a0, 19 December 1984.

Aumann, H. H. and Ruzmaikin, A.: Frequency of deep convective clouds in the tropical zone from 10 years of AIRS data, Atmos. Chem. Phys., 13, 10795–10806, 2013.

Barret, B., Williams, J. E., Bouarar, I., Yang, X., Josse, B., Law, K., Pham, M., Flochmoen, E. Le, Liousse, C., Peuch, V.H., Calver, G.D., Pyle, J.A., Sauvage ,B., Velthoven P. van and Schlager, H.: Impact of West African Monsoon convective transport and lightning NO_x production upon the upper tropospheric composition: a multi-model study, Atm. Chem. Phys., **10**, 5719-5738, doi:10.5194/acp-10-5719-2010, 2010.

Barret B., Ricaud P., Mari C., Attie´ J.-L., Bousserez N., Josse B., Flochmoen E. LeLivesey N. J., Massart S., Peuch V.-H., , Piacentini A., Sauvage B., Thouret V., and Cammas J.-P. Transport pathways of CO in the African upper troposphere during the monsoon season: a study based upon the assimilation of spaceborne observations, Atmos. Chem. Phys., 8, 3231–3246, 2008.

753 Barth, M., Lee, C, J., Hodzic, A. Pfister, G., Skamarock, W. C., Worden, J. , Wong, J., and
754 Noone, D.: Thunderstorms and upper troposphere chemistry during the early stages of the
755 2006 North American Monsoon, Atmos. Chem. Phys., 12, 11003–11026, 2012.
756 Bouarar, I., Law, K. S., Pham, M., Liousse, C., Schlager, H., Hamburger, T., Reeves, C. E.,
757 Cammas, J.-P., Ned´ el´ ec´ P., Szopa, S, Ravegnani, F., Viciani, S., D'Amato F.,
758 Ulanovsky A., and Richter A.: Emission sources contributing to tropospheric ozone over
759 Equatorial Africa during the summer monsoon, Atmos. Chem. Phys., 11, 13395–13419,
760 doi:10.5194/acp-11-13395-2011, 2011.
761 Carmichael, G. R., Tang Y., Kurata G., Uno I., Streets D., Woo J.-H.,
762 Huang H., Yienger J., Lefer B., Shetter R., Blake D., Atlas E., Fried
763 A., Apel E., Eisele F., Cantrell C., Avery M., Barrick J., Sachse G.,
764 Brune W., Sandholm S., Kondo Y., Singh H., Talbot R., Bandy A.,
765 Thorton D., Clarke A., and Heikes B., Regional-scale chemical
766 transport modeling in support of the analysis of observations obtained
767 during the TRACE-P experiment, J. Geophys. Res., 108(D21), 8823,
768 doi:10.1029/2002JD003117, 2003.
769 CEC (Commission for Environmental Cooperation) report on North American Power Plant Air
770 Emissions, IBSN : 978-2-89700-008-0,October 2011.
771 Chang, Chih-Pei, Ding Y., Lau, Gabriel Ngar-Cheung, Johnson, R. H, Wang, B., and Yasunari,
772 T.: The Global Monsoon System: Research and Forecast (2nd Edition) edited by Chih-
773 Pei Chang et al., World Scientific Publishing Co, 2011.
774 Choi, Y., Kim, J., Eldering, A., Osterman, G., Yung, Y. L., Gu, Y., and Liou, K. N.: Lightning
775 and anthropogenic NO_x sources over the United States and the western North Atlantic

776 Ocean: impact on OLR and radiative effects, Geophys. Res. Lett., 36, L17806,
777 doi:10.1029/2009GL039381, 2009.
778 Collier J.C. and Zhang G.J.: Simulation of the North American Monsoon by the NCAR CCM3
779 and Its Sensitivity to Convection Parameterization, J. of Clim., 2851-2866, 2006.
780 Cooper, O. R., Eckhardt, S., Crawford, J. H., Brown, C. C., Cohen, R. C., Bertram, T. H.,
781 Wooldridge, P., Perring, A., Brune, W.H., Ren, X., Brunner, D., and Baughcum, S. L.:
782 Summertime buildup and decay of lightning NO_x and aged thunderstorm outflow above
783 North America, J. Geophys.Res., 114, D01101, doi:10.1029/2008JD010293, 2009.
784 Dickerson, R. R., Huffman, G. J., Luke, W. T., Nunnermacker, L. J., Pickering, K. E. , Leslie,
785 A., Lindsey, C., Slinn, W., Kelly, T., Daum, P., Delany, A., Grennberg, J., Zimmerman,
786 P., Boatman, J., Ray, J., and Stedman, D.: Thunderstorms: An important mechanism in
787 the transport of air pollutants, Science, 235, 460 – 465, 1987.
788 Dong, L. and Colucci, S. J. : The Role of Deformation and Potential Vorticity in Southern
789 Hemisphere Blocking Onsets, J. Atmos. Sci., 62, 4043-4056, 2005.
790 Drummond, J. W., D. H. Ehhalt, and A. Volz, Measurements of nitric oxide between 0 – 12
791 km altitude and 67 N-60 S latitude obtained during STRATOZ III, J. Geophys. Res,
792 93, 15,831 – 15,849, 1988.
793 Emmons, L. K., Hauglustaine, D. A., Muller, J.-F., Carroll, M. A., Brasseur, G. P., Brunner, D.,
794 Staehelin, J., Thouret, V., and Marenco, A.: Data composites of tropospheric ozone and
795 its precursors from aircraft measurements, J. Geophys. Res., 105, 20,497 – 20,538, 2000.
796 Evett, R. R., Mohrle C. R., Hall B. L., Brownb T. J. and Stephens S. L.: The effect of monsoonal
797 atmospheric moisture on lightning fire ignitions in southwestern North America,
798 Agricultural and forest meteorology, 148, 1478–1487, 2008.

Fadnavis, S., Semeniuk, K., Pozzoli, L., Schultz, M. G., Ghude, S. D., Das, S. and Kakatkar, R.: Transport of aerosols into the UTLS and their impact on the Asian monsoon region as seen in a global model simulation, Atmos. Chem. Phys., 13, 8771–8786, 2013, doi:10.5194/acp-13-8771-2013.Fadnavis S, Schultz M. G., Semeniuk K., Mahajan A. S., Pozzoli L., Sonbawne S., Ghude S. D., Kiefer M., and Eckert E., Trends in Peroxyacetyl Nitrate (PAN) in the Upper Troposphere and Lower Stratosphere over Southern Asia during the summer monsoon season: Regional Impacts, Atmos. Chem. Phys., 14, 12725–12743, doi:10.5194/acp-14-12725-2014, 2014.

Fiore, A. M., Horowitz, L. W., Purves, D. W., Levy II, H., Evans, M. J., Wang, Y., Li, Q., and Yantosca, R. M.: Evaluating the contribution of changes in isoprene emissions to surface ozone trends over the eastern United States, J. Geophys. Res., 110, D12303, doi:10.1029/2004JD005485, 2005.

Fischer E. V., Jacob D. J., Yantosca R. M., Sulprizio M. P., Millet D. B., Mao J., Paulot F., Singh H. B., Roiger A., Ries L., Talbot R.W., Dzepina K., and Pandey Deolal S., Atmospheric peroxyacetyl nitrate (PAN): a global budget and source attribution, Atmos. Chem. Phys., 14, 2679–2698, doi:10.5194/acp-14-2679-2014, 2014.

Fischer, H. and Oelhaf, H.: Remote sensing of vertical profiles of atmospheric trace constituents with MIPAS limb-emission spectrometers, Appl. Optics, 35, 2787–2796, 1996.

Fischer, H., Birk, M., Blom, C., Carli, B., Carlotti, M., von Clarmann, T., Delbouille, L., Dudhia, A., Ehhalt, D., Endemann, M., Flaud, J. M., Gessner, R., Kleinert, A., Koopman, R., Langen, J., Lopez-Puertas, M., Mosner, P., Nett, H., Oelhaf, H., Perron, G., Remedios, J., Ridolfi, M., Stiller, G., and Zander, R.: MIPAS: an instrument for atmospheric and climate research, Atmos. Chem. Phys., 8, 2151–2188, 2008, doi:10.5194/acp-8-2151-2008.

823 Fu, R., Hu, Y., Wright, J. S., Jiang, J. H., Dickinson, R. E., Chen, M., Filipiak, M., Read, W. G.,
824 Waters, J.W. and Wu, D. L.: Short circuit of water vapour and polluted air to the global
825 stratosphere by convective transport over the Tibetan Plateau, Proc Natl Acad Sci U S A.
826 Apr 11, 103(15), 5664-9, Epub Apr 3, 2006.
827 Galanter, M., H. Levy II, and G. R. Carmichael (2000), Impacts of biomass burning on
828 tropospheric CO, NO_x, and O_3, J. Geophys. Res., 105(D5), 6633–6653,
829 doi:10.1029/1999JD901113.
830 Ganzeveld, L., and Lelieveld, J.: Dry deposition parameterization in a chemistry general
831 circulation model and its influence on the distribution of reactive trace gases, J. Geophys.
832 Res.,100(D10), 20999–21012, doi:10.1029/95JD02266, 1995.
833 Garny, H., and Randel, W. J.: Dynamic variability of the Asian monsoon anticyclone observed in
834 potential vorticity and correlations with tracer distributions, J. Geophys. Res. Atmos.,
835 118, 13,421–13,433, doi:10.1002/2013JD020908, 2013.
836 Gettelman, A., Salby, M. L., and Sassi, F.: Distribution and influence of convection in the
837 tropical tropopause region, J. Geophys. Res., 107(D10), 4080,
838 doi:10.1029/2001JD001048, 2002.
839 Gettelman, A., Hoor, P., Pan, L. L., Randel, W. J., Hegglin, M. I., and Birner, T.: The
840 extratropical upper troposphere and lower stratosphere, Rev. Geophys., 49, RG3003,
841 doi:10.1029/2011RG000355, 2011.
842 Glatthor, N., Clarmann, T. von, Fischer, H., Funke, B., Grabowski, U., Höpfner, M., Kellmann,
843 S., Kiefer, M., Linden, A., Milz M., Steck, T., and Stiller, G.P.: Global peroxyacetyl
844 nitrate (PAN) retrieval in the upper troposphere from limb emission spectra of the
845 Michelson Interferometer for Passive Atmospheric Sounding (MIPAS), Atmos. Chem.
846 Phys., 7, 2775-2787, www.atmos-chem-phys.net/7/2775/2007/ doi:10.5194/acp-7-2775-
847 2007, 2007.

Grewe, V., Brunner, D., Dameris, M. , Grenfell, J.L., Hein, R., Shindell, D. and Staehelin, J. : Origin and Variability of Upper Tropospheric Nitrogen Oxides and Ozone at Northern Mid-Latitudes. Atmos. Environ., 35, 3421-3433, 2001.

Harris, R. C., et al., The Amazon boundary layer experiment (ABLE 2A) dry season 1985, J. GeOphys. Res., 93, 1351-1360, 1988.

Harriss, R.C., S.C. Wofsy, D.S. Bartlett, M.C. Shipham, D.J. Jacob, J.M. Hoell, Jr., R.J. Bendura, J.W. Drewry, R.J. McNeal, R.L. Navarro, R.N. Gidge, and V.E. Rabine, The Arctic Boundary Layer Expedition (ABLE 3A): July-August 1988, J. Geophys. Res., 97, 16,383-16,394, 1992.

Harriss, R.C., S.C. Wofsy, J.M. Hoell, Jr., R.J. Bendura, J.W. Drewry, R.J. McNeal, D. Pierce, V.Rabine, and R.L. Snell, The Arctic Boundary Layer Expedition (ABLE-3B): July-August 1990, J. Geophys. Res., 99, 1635-1643, 1994.

Hassim, M. E. E., Lane, T. P., and May, P. T.: Ground-based observations of overshooting convection during the Tropical Warm Pool-International Cloud Experiment, J. Geophys. Res. Atmos.,119, 880–905, doi:10.1002/2013JD020673, 2014.

Hoell, J. M., Jr., D. L. Albritton, G. L. Gregory, R. J. McNeal, S. M. Beck, R. J. Bendura, and J. W. Drewry, Operational overview of NASA GTE/CITE 2 airborne instrumentintercomparisons: Nitrogen dioxide, nitric acid, and peroxyacetyl nitrate, J. Geophy. Res., 95, 10,047-10,054, 1990.

Hoell, J. M., Jr., D. L. Albritton, G. L. Gregory, R. L. McNeal, S. M. Beck, R. J. Bendura, and J, W. Drewry, Operational overview of NASA GTE/CITE-2 airborne instrument intercomparison: Nitrogen dioxide, nitric acid, and peroxyacetyl nitrate. *J. Geophy. Res*., *95*, 10,047-10,054, 1990

Horowitz, L. W., Walters, S., Mauzerall, D. L., Emmons, L. K., Rasch, P. J., Granier, C., Tie, X., Lamarque, J., Schultz, M. G.,Tyndall, G. S., Orlando, J. J. and Brasseur, G. P.: A global simulation of tropospheric ozone and related tracers, Description and evaluation of MOZART, version 2, J. Geophys. Res.,108(D24), 2003.

875 Hudman, R. C., Jacob, D. J., Cooper, O. R., Evans, M. J., Heald, C. L., Park, R. J., Fehsenfeld,
876 F., Flocke, F., Holloway, J., Hübler, G., Kita, K., Koike, M., Kondo, Y., Neuman, A.,
877 Nowak, J., Oltmans, S., Parrish, D., Roberts, J. M., and Ryerson, T.: Ozone production in
878 transpacific Asian pollution plumes and implica tions for ozone air quality in California, J.
879 Geophys. Res., 109, D23S10, doi:10.1029/2004jd004974, 2004.

880 Hudman, R. C., Jacob, D. J., Turquety, S., Leibensperger, E. M., Murray, L. T., Wu, S.,
881 Gilliland, A. B., Avery, M., Bertram,T. H., Brune, W., Cohen, R. C., Dibb, J. E., Flocke,
882 F. M.,Fried, A., Holloway, J., Neuman, J. A., Orville, R., Perring, A.,Ren, X., Ryerson,
883 T. B., Sachse, G. W., Singh, H. B., Swanson, A., and Wooldridge, P. J.: Surface and
884 lightning sources of nitrogen oxides over the United States: magnitudes, chemical
885 evolution, and outflow, J. Geophys. Res., 112, D12S05, doi:10.1029/2006JD007912,
886 2007.

887 Keim, C., Liu, G. Y. , Blom, C.E., Fischer, H., Gulde, T., Höpfner, M., Piesch, C., Ravegnani,
888 F., Roiger, A., Schlager, H., and Sitnikov, N.: Vertical profile of peroxyacetyl nitrate (PAN)
889 from MIPAS-STR measurements over Brazil in February 2005 and its contribution to
890 tropical UT NO_y partitioning, Atmos. Chem. Phys., 8, 4891-4902, doi:10.5194/acp-8-4891-
891 2008, 2008.

892 Khaykin S., Pommereau, J.-P., Korshunov, L., Yushkov, V., Nielsen, J., Larsen, N.,
893 Christensen, T., Garnier, A., Lukyanov, A., and Williams, E.: Hydration of the lower
894 stratosphere by ice crystal geysers over land convective systems, Atmos. Chem. Phys., 9,
895 2275–2287, 2009.

896 Kulkarni J.R., Maheshkumar, R.S., Morwal, S.B., Padma kumari, B., Konwar, M., Deshpande,
897 C.G., Joshi, R.R., Bhalwankar, R.V., Pandithurai, G., Safai, P.D., Narkhedkar, S.G.,

898 Dani, K.K., Nath, A., Nair, Sathy, Sapre, V.V., Puranik, P.V., Kandalgaonkar, S.S.,
899 Mujumdar, V.R., Khaladkar, R.M., Vijaykumar, R., Prabha, T.V., Goswami, B.N., The
900 Cloud Aerosol Interaction and Precipitation Enhancement Experiment (CAIPEEX):
901 overview and preliminary results (2012), Curr. Sci., Vol.102, 2012, 413-425.

902 Labrador, L. J., Kuhlmann, R. von, and Lawrence, M. G.: The effects of lightning-produced
903 NO_x and its vertical distribution on atmospheric chemistry: sensitivity simulations with
904 MATCH-MPIC, Atmos. Chem. Phys., 5, 1815–1834, 2005.

905 Lamsal, L. N., Martin, R. V., Padmanabhan, A., van Donkelaar, A., Zhang, Q., Sioris, C. E.,
906 Chance, K., Kurosu, T. P., and Newchurch, M. J.: Application of satellite observations
907 for timely updates to global anthropogenic NO_x emission inventories, Geophys. Res.
908 Lett., 38,L05810, doi:10.1029/2010GL046476, 2011.

909 Li, Q., Jiang, J. H., Wu, D. L., Read, W. G., Livesey, N. J., Waters, J. W., Zhang, Y., Wang, B.,
910 Filipiak, M. J., Davis, C. P., Turquety, S., Wu, S., Park R. J., Yantosca R. M., and Jacob
911 D. J.: Convective outflow of South Asian pollution: A global CTM simulation compared
912 with EOS MLS observations, Geophys. Res. Lett., 32, L14826,
913 doi:10.1029/2005GL022762, 2005.

914 Liang, Q., Rodriguez, J. M., Douglass, A. R., Crawford, J. H., Olson, J. R., Apel, E., Bian, H.,
915 Blake, D. R., Brune, W., Chin, M., Colarco, P. R., da Silva, A., Diskin, G. S.,
916 Duncan, B. N., Huey, L. G., Knapp, D. J., Montzka, D. D., Nielsen, J. E., Pawson, S.,
917 Riemer, D. D., Weinheimer, A. J., and Wisthaler, A.: Reactive nitrogen, ozone and ozone
918 production in the Arctic troposphere and the impact of stratosphere-troposphere
919 exchange, Atmos. Chem. Phys., 11, 13181-13199, doi:10.5194/acp-11-13181-2011,
920 2011.

921 Liu, C., and Zipser E. J.: Global distribution of convection penetrating the tropical tropopause, J.
922 Geophys. Res., 110, D23104, 2005.

923 Martin, R. V., Sauvage, B., Folkins, I., Sioris, C. E., Boone, C., Bernath, P., and Ziemke, J.:
924 Space-based constraints on the production of nitric oxide by lightning, J. Geophys. Res.,
925 112, D09309, doi:10.1029/2006JD007831, 2007.
926 Miyazaki, K., Eskes, H. J., and Sudo, K.: Global NO_x emission estimates derived from an
927 assimilation of OMI tropospheric NO2 columns, Atmos. Chem. Phys., 12, 2263–2288,
928 doi:10.5194/acp-12-2263-2012, 2012.
929 Murray, L. T., Jacob, D. J., Logan, J. A., Hudman, R. C., and Koshak, W. J.: Optimized regional
930 and interannual variability of lightning in a global chemical transport model constrained
931 by LIS/OTD satellite data, J. Geophys. Res., 117, D20307, doi:10.1029/2012JD017934,
932 2012.
933 O'Sullivan D. W., • Heikes B. GLee., M., Chang W., Gregory G. L., • Blake D. R., and Sachs
934 G. W., Distribution of hydrogen peroxide and methylhydroperoxide over the Pacific and
935 South Atlantic Oceans, *J. Geophys. Res*, 104, D5, 5635-5646, 1999.
936 Pan L. L., A. Kunz, C. R. Homeyer , L. A. Munchak, D. E. Kinnison , and S. Tilmes,
937 Commentary on using equivalent latitude in the upper troposphere and lower
938 stratosphere, Atmos. Chem. Phys., 12, 9187–9199, doi:10.5194/acp-12-9187-2012 ,
939 2012,
940 Park M., Randel W. J., Getteleman, A., Massie, S. T., and Jiang, J. H.: Transport above the
941 Asian summer monsoon anticyclone inferred from Aura Microwave Limb Sounder
942 tracers, J. Geophys. Res., 112, D16309, doi:10.1029/2006JD008294, 2007.
943 Park, M., Randel, W. J., Emmons, L. K., and Livesey, N. J.: Transport pathways of carbon
944 monoxide in the Asian summer monsoon diagnosed from Model of Ozone and Related
945 Tracers (MOZART), J. Geophys. Res., 114, D08303, doi:10.1029/2008JD010621, 2009.

946 Park, M., Randel, W. J., Kinnison, D. E., Garcia, R. R., and Choi, W.: Seasonal variation of
947 methane, water vapour, and nitrogen oxides near the tropopause: Satellite observations
948 and model simulations, J. Geophys. Res., doi:10.1029/2003JD003706, 109, D03302,
949 2004.
950 Penki, R. K. and Kamra, A. K.: Lightning distribution with respect to the monsoon trough
951 position during the Indian summer monsoon season, J. Geophy. Res., 118, 4780–4787,
952 doi:10.1002/jgrd.50382, 2013.
953 Pozzoli, L., Bey, I., Rast, J. S., Schultz, M. G., Stier, P., and Feichter, J.: Trace gas and aerosol
954 interactions in the fully coupled model of aerosol-chemistry-climate ECHAM5-
955 HAMMOZ: 1. Model description and insights from the spring 2001 TRACE-P
956 experiment, J. Geophys. Res., 113, D07308, doi:10.1029/2007JD009007, 2008a.
957 Pozzoli, L., Bey, I., Rast, J. S., Schultz, M. G., Stier, P., and Feichter, J.: Trace gas and aerosol
958 interactions in the fully coupled model of aerosol-chemistry-climate ECHAM5-
959 HAMMOZ: 2. Impact of heterogeneous chemistry on the global aerosol distributions, J.
960 Geophys. Res., 113, D07309, doi:10.1029/2007JD009008, 2008b.
961 Pozzoli, L., Janssens-Maenhout, G., Diehl, T., Bey, I., Schultz, M. G., Feichter, J., Vignati, E.,
962 and Dentener, F.: Re-analysis of tropospheric sulfate aerosol and ozone for the period
963 1980–2005 using the aerosol-chemistry-climate model ECHAM5-HAMMOZ, Atmos.
964 Chem. Phys., 11, 9563-9594, doi:10.5194/acp-11-9563-2011, 2011.
965 Prabha T.V., Khain A., Maheshkumar R.S., Pandithurai G., Kulkarni J.R., Goswami B.N.
966 (2011),Microphysics of Premonsoon and Monsoon Clouds as Seen from In Situ
967 Measurements during the Cloud Aerosol Interaction and Precipitation Enhancement
968 Experiment (CAIPEEX), **J. Atm. Sc.**, Vol.68 , 2011, DOI: 10.1175/2011JAS3707.1,
969 1882-1901
970 Price, C. and Asfur, M.: Inferred long term trends in lightning activity over Africa, Earth Planets
971 Space, 58, 1197–1201, 2006.
972 Ranalkar, M. R and Chaudhari, H. S.**:** Seasonal variation of lightning activity over the Indian
973 subcontinent. *Meteorology and Atmospheric Physics*. 104, 125–134, 2009.

974 Randel, W. J. and Park, M.: Deep convective influence on the Asian summer monsoon
975 anticyclone and associated tracer variability observed with Atmospheric Infrared Sounder
976 (AIRS), J. Geophys. Res., 111, D12314, doi:10.1029/2005JD006490, 2006.
977 Randel, W. J., Moyer, E., Park, M., Jensen, E., Bernath, P., Walker, K., and Boone C.: Global
978 variations of HDO and HDO/H2O ratios in the upper troposphere and lower stratosphere
979 derived from ACE-FTS satellite measurements, J. Geophys. Res., 117, D06303,
980 doi:10.1029/2011JD016632, 2012.
981 Randel, W. J., Park, M., Emmons, L., Kinnison, D., Bernath, P., Walker, K. A., Boone, C. and
982 Pumphrey H.: Asian monsoon transport of pollution to the stratosphere, Science. Apr
983 30,328(5978),611-3. Epub Mar 25, 2010.
984 Rast, S., M.G. Schultz, I. Bey, T. van Noije and co-authors, Evaluation of the tropospheric
985 chemistry general circulation model ECHAM5–MOZ and its application to the analysis
986 of the chemical composition of the troposphere with an emphasis on the late RETRO
987 period 1990–2000 Technical rapport: 2014, Max Planck Institute of Meteorology, Earth
988 System Science, 74p. Real, E., Orlandi, E., Law, K. S., Fierli, F., Josset, D., Cairo, F.,
989 Schlager, H., Borrmann, S., Kunkel, D., Volk, C. M., McQuaid, J. B., Stewart, D. J., Lee,
990 J., Lewis, A. C., Hopkins, J. R., Ravegnani, F., Ulanovski A. and Liousse C.: Cross-
991 hemispheric transport of central African biomass burning pollutants: implications for
992 downwind ozone production, Atmos. Chem. Phys., 10, 3027–3046, 2010.
993 Ridley, B. A., Madronich, S., Chatfield, R. B., Walega, J. G., Shetter, R. E., Carroll, M. A.,
994 and Montzka D. D: Measurements and model simulations of the photostationary state
995 during the Mauna Loa Observatory Photochemistry Experiment: Implications for radical
996 concentrations and ozone production and loss rates, J. Geophys. Res., 97(D10), 10375–
997 10388, doi:10.1029/91JD02287, 1992.

998 Ridley, B.A., J.G. Walega, J.E. Dye, and F.E. Grahek, Distributions of NO, NO_x, NO_y, and O_3 to
999 12 km altitude during the summer monsoon season over New Mexico, *J. Geophys. Res.*,
1000 *99*, 25,519-25,534, 1994.
1001 Roeckner, E., Bauml, G., Bonaventura, L., Brokopf, R., Esch, M., Giorgetta, M., Hagemann, S.,
1002 Kirchner, I., Kornblueh, L., Manzini, E., Rhodin, A., Schlese, U., Schulzweida, U., and
1003 Tompkins, A.: The atmospehric general circulation model ECHAM5: Part 1, Tech. Rep.
1004 349, Max Planck Institute for Meteorology, Hamburg, 2003.
1005 Sander, S. P. Fried, R. R., Barker, J. R., Golden,D. M., Kurylo, M. J. , Wine, P. H., J. Abbatt P.
1006 D., Burkholder, J. B., Kolb, C. E., Moortgat, G. K., Huie, R. E., Orkin, V. L.: Chemical
1007 kinetics and photochemical data for use in atmospheric studies, evaluation number 14,
1008 JPL Publ. 02-25, Jet Propul. Lab., Calif. Inst. of Technol., Pasadena. (Available
1009 at http://jpldataeval.jpl.nasa.gov/pdf/JPL_02-25_rev02.pdf), 2003.
1010 Schmitz, J. T., Mullen S. L., 1996: Water Vapor Transport Associated with the Summertime
1011 North American Monsoon as Depicted by ECMWF Analyses. J. Climate, **9**, 1621–1634.,
1012 1996.
1013 Schultz, M., Backman, L., Balkanski, Y., Bjoerndalsaeter, S., Brand, R., Burrows, J., Dalsoeren,
1014 S., de Vasconcelos, M., Grodtmann, B., Hauglustaine, D., Heil, A., Hoelzemann, J.,
1015 Isaksen, I., Kaurola, J., Knorr, W., Ladstaetter-Weienmayer, A., Mota, B., Oom, D.,
1016 Pacyna, J., Panasiuk, D., Pereira, J., Pulles, T., Pyle, J., Rast, S., Richter, A., Savage, N.,
1017 Schnadt, C., Schulz, M., Spessa, A., Staehelin, J., Sundet, J., Szopa, S., Thonicke, K., van
1018 het Bolscher, M., van Noije, T., van Velthoven, P., Vik, A., and Wittrock, F.: REanalysis
1019 of the TROpospheric chemical composition over the past 40 years (RETRO). A long-
1020 term global modeling study of tropospheric chemistry. Final Report, Tech. rep., Max
1021 Planck Institute for Meteorology, Hamburg, Germany, 2007.

1022 Schultz, M. G., Heil, A., Hoelzemann, J. J., Spessa, A., Thonicke, K., Goldammer, J. G., Held,
1023 A. C., Pereira, J. M. C., and van het Bolscher, M.: Global wildland fire emissions from
1024 1960 to 2000, Global Biogeochem. Cy., 22, GB2002, doi:10.1029/2007GB003031, 2008

1025 Schultz, M.G., T. Pulles, R. Brand, M. Van het Bolscher and S.T. Dalsøren, , A global data set of
1026 anthropogenic CO, NO_x, and NMVOC emissions for 1960-2000, in preparation and
1027 available at http://eccad.sedoo.fr/

1028 Schultz, M.G, A. Heil, J.J. Hoelzemann, A. Spessa, K. Thonicke, J. Goldammer, A.C. Held, J.M.
1029 Pereira, M. Van Het Bolscher, 2005: Global Wildland Fire Emissions from 1960 to 2000,
1030 doi:10.1029/2007GB003031 , Global Biogeochemical Cycles 22 (GB2002) : 17 PP

1031 Schumann, U. and Huntrieser, H.: The global lightning-induced nitrogen oxides source, Atmos.
1032 Chem. Phys., 7, 3823–3907, 2007.

1033 Shepon, A., Gildor, H., Labrador, L. J., Butler, T., Ganzeveld, L. N., and Lawrence, M. G.:
1034 Global reactive nitrogen deposition from lightning NO_x, J. Geophys. Res., 112, D06304,
1035 doi:10.1029/2006JD007458, 2007.

1036 Singh, H. B., Viezee, W., Chen, Y., Thakur, A. N., Kondo, Y. and Talbot, R. W.,Gregory, G. L.,
1037 Sachse, G. W., Blake, D. R., Bradshaw, J. D., Wang, Y., and Jacob D. J.: Latitudinal
1038 distribution of reactive nitrogen in the free troposphere over the Pacific Ocean in late
1039 winter/early spring, J. Geophys. Res., 103(D21), 28237–28246, doi:10.1029/98JD01891,
1040 1998.

1041 Singh, H. B.,Reactive nitrogen in the troposphere, Environ. Sci. Technol., 21(4), 320–327, 1987

1042 Singh, H.B., Salas, L.J. and Viezee, W.: Global distribution of peroxyacetyl nitrate, Nature, Jun
1043 5-11;321(6070):588-91, 1986.
1044 Singh, H. B., Brune W. H., Crawford J. H., Jacob D. J., and Russell P. B.: Overview of the
1045 summer 2004 Intercontinental Chemical Transport Experiment – North America
1046 (INTEX-A), J. Geophys. Res., 111, 2006, D24S01, doi:10.1029/2006JD007905.
1047 Stier, P., Feichter, J., Kinne, S., Kloster, S., Vignati, E., Wilson, J., Ganzeveld, T., Tegen, I.,
1048 Werner, M., Balkanski, Y., Schulz, M., Boucher, O., Minikin, A., and Petzold, A.: The
1049 aerosol climate model ECHAM5-HAM, Atmos. Chem. Phys. 5, 1125– 1165,
1050 doi:10.5194/acp-5-1125-2005, 2005.
1051 Talbot, R. W., Dibb, J. E., Scheuer, E. M., Bradshaw, J. D., Sandholm, S. T., Singh, H. B.,
1052 Blake, D. R., Blake, N. J., Atlas, E., and Flocke, F.: Tropospheric reactive odd nitrogen
1053 over the South Pacific in austral springtime, J. Geophys. Res., 105, 6681–6694,
1054 doi:10.1029/1999JD901114, 2000.
1055 Talukdar, R. K., Burkholder, J. B., Schmoltner, A., Roberts, J. M., Wilson, R. R. and
1056 Ravishankara, A. R.: Investigation of loss processes for peroxyacetyl nitrate in the
1057 atmosphere: UV photolysis and reaction with OH, J. Geophys. Res., 100, 14163–14173,
1058 1995.
1059 Tang, J. H., Chan, L. Y., Chang, C. C., Liu, S., and Li, Y. S.: Characteristics and sources of non-
1060 methane hydrocarbons in background atmospheres of eastern, southwestern, and southern
1061 China, J. Geophys. Res., 114, D03304, doi:10.1029/2008JD010333, 2009.
1062 Tereszchuk K. A., Moore D. P., Harrison J. J., Boone C. D., Park M., Remedios J. J., Randel W.
1063 J., and Bernath P. F., Observations of peroxyacetyl nitrate (PAN) in the upper
1064 troposphere by the Atmospheric Chemistry ExperimentFourier Transform Spectrometer
1065 (ACE-FTS), Atmos. Chem. Phys., 13, 5601–5613, doi:10.5194/acp-13-5601-2013, 2013.
1066 Tie, X.X., Zhang, R., Brasseur, G., Emmons, L. and Lei, W.: Effects of lightning on reactive
1067 nitrogen and nitrogen reservoir species in the troposphere. *Journal of Geophysical*
1068 *Research-Atmospheres*, **106**, 3167-3178, DOI: 10.1029/2000JD900565, 2001.

1069 Uppala S. M., KÅllberg P. W., Simmons A. J.,*, Andrae U., Costa Bechtold V. Da, Fiorino
1070 M., Gibson J. K., Haseler J., Hernandez A., Kelly G. A., Li X., Onogi K., Saarinen
1071 S., Sokka N., Allan R. P., Andersson E., Arpe K., Balmaseda M. A., Beljaars A. C.
1072 M., Berg L. Van De, Bidlot J., Bormann N., Caires S., Chevallier F., Dethof A.,
1073 Dragosavac M., Fisher M., Fuentes M., Hagemann S., Hólm E., Hoskins B. J.,
1074 Isaksen L., Janssen P. A. E. M., Jenne R., Mcnally A. P., Mahfouf J.-F., Morcrette J.-
1075 J., Rayner N. A., Saunders R. W., Simon P., Sterl A., Trenberth K. E., Untch A.,
1076 Vasiljevic D., Viterbo P. and Woollen J.,

1077 The ERA-40 re-analysis, Q. J. R. Meteorol. Soc., 131(612), 2961–3012, doi:10.1256/qj.04.176,
1078 2005.

1079 Vaughan G. and Timmis C.: Transport of near-tropopause air into the lower midlatitude
1080 stratosphere, Q. J. R. Meteorol. SOC., 124, pp. 1559-1578, 1998.

1081 Von Clarmann, T., Höpfner, M., Kellmann, S., Linden, A., Chauhan, S., Funke, B., Grabowski,
1082 U.,Glatthor, N., Kiefer, M., Schieferdecker, T., Stiller, G. P., and Versick, S.: Retrieval of
1083 temperature, H2O, O3, HNO_3, CH_4, N_2O, $ClONO_2$ and ClO from MIPAS reduced
1084 resolution nominal mode limb emission measurements, Atmos. Meas. Tech., 2, 159–175,
1085 doi:10.5194/amt-2- 2159-2009, 2009.

1086 Wiegele A., Glatthor N., Hopfner M., Grabowski U., Kellmann S., Linden A., Stiller G., and von
1087 Clarmann T.: Global distributions of C_2H_6, C_2H_2, HCN, and PAN retrieved from MIPAS
1088 reduced spectral resolution measurements, Atmos. Meas. Tech., 5, 723–734,
1089 doi:10.5194/amt-5-723-2012, 2012,

1090 Xiong, X., Houweling, S., Wei, J., Maddy, E., Sun, F., and Barnet, C.: Methane plume over
1091 South Asia during the monsoon season: Satellite observation and model simulation,
1092 Atmos. Chem. Phys., 9, 783– 794, 2009.

1093 Zhang, L, Jacob, D. J., Boersma, K. F., Jaffe, D. A., Olson, J. R., Bowman, K. W., Worden, J.
1094 R., Thompson, A. M., Avery, M. A., Cohen, R. C., Dibb, J. E., Flock, F. M., Fuelberg, H.
1095 E., L. Huey, G., McMillan, W.W., Singh, H. B., and Weinheimer, A. J.: Transpacific
1096 transport of ozone pollution and the effect of recent, Asian emission increases on air

quality in North America: an integrated analysis using satellite, aircraft, ozonesonde, and surface observations, Atmos. Chem. Phys., 8, 6117–6136, 2008.

Zhao, C., Wang, Y., Choi, Y., and Zeng, T.: Summertime impact of convective transport and lightning NO_x production over North America: modeling dependence on meteorological simulations, Atmos. Chem. Phys., 9, 4315–4327, 2009.

Ziereis, H., H. Schlager, P. Schulte, P.F.J. van Velthoven, and F. Slemr, Distributions of NO, NO_x, and NO_y in the upper troposphere and lower stratosphere between 28°N and 61°N during POLINAT 2, *J. Geophys. Res.*, **105**, 3653, 2000.

1107 Table 1: Global aircraft measurements used for model evaluation.

Experiment	Date Frame	Species	Location
POLINAT-2 (Falcon) Ziereis et al.2000	Sep 19-Oct 25, 1997	O_3, NO_x	Canary-Islands: LAT= 25^{O}N, 35^{O}N, LON=160^{O}W, 170^{O}W E-Atlantic: LAT= 35^{O}N, 45^{O}N, LON=150^{O}W,160^{O}W Europe: LAT= 45^{O}N, 55^{O}N, LON=5^{O}E, 15^{O}E Ireland: LAT=50^{O}N, 60^{O}N, LON= 165^{O}W,175^{O}W
PEM-Tropics-A (DC8) Talbot et al. (2000)	Aug 24-Oct 15, 1996	O_3, NO_x, HNO_3, PAN	Christmas-Island: LAN= 0^{O}, 10^{O}N, LON=20^{O}W, 40^{O}W Easter-Island: LAT=-40^{O}N, 20^{O}S, LON=60^{O}W, 80^{O}W Fiji: LAT= 0^{O},10^{O}S. LON= 170^{O}E, 10^{O}W lawaii: LAT= 10^{O}N, 30^{O}N, LON= 10^{O}W., 30^{O}W Tahiti: LAT= 20^{O}S, 0^{O}, LON= 20^{O}W, 50^{O}W
PEM-Tropics-A (P3) O'Sullivan et al, 1999	Aug 15-Sep 26, 1996	O_3, HNO_3	Christmas-Island: LAT= 0^{O}, 10^{O}N, LON= 20^{O}W, 40^{O}W Easter-Island: LAT= 40^{O}S, 20^{O}S, LON= 60^{O}W, 80^{O}W Hawaii: LAT= 10^{O}N, 30^{O}N, LON= 10^{O}W, 30^{O}W Tahiti: LAT= 20^{O}S, 0^{O}, LON= 20^{O}W, 50^{O}W
ABLE-3B (Electra) Harriss et al.,1994	Jul 6-Aug 15, 1990	O_3, NO_x, HNO_3, PAN	Labrador: LAT= 50^{O}N, 55^{O}N, LON= 120^{O}W, 135^{O}W Ontario: LAT= 45^{O}N, 60^{O}N, LON= 90^{O}W, 100^{O}W US-E-Coast: LAT= 35^{O}N, 45^{O}N, LON= 100^{O}W, 110^{O}W.
CITE-3 (Electra) Hoell et al 1993	Aug 22-Sep 29, 1989	O_3, NO_x	Natal: LAT= 15^{O}S.,5^{O}N, LON= 145^{O}W, 155^{O}W Wallops: LAT= 30^{O}N, 40^{O}N, LON= 100^{O}W, 110^{O}W
ELCHEM (Sabreliner) Ridley et al.,1999	Jul 27-Aug 22, 1989	O_3, NO_x	New-Mexico: LAT=30^{O}N, 35^{O}N , LON= 70^{O}W, 75^{O}W
ABLE-3A (Electra) Harriss et al.,1992	Jul 7-Aug 17, 1988	O_3, NO_x ,PAN	Alaska: LAT= 55^{O}N, 75^{O}N, LON= 10^{O}W, 25^{O}W
ABLE-2A (Electra) Harris et al., 1988	Jul 12-Aug 13, 1985	O_3	E-Brazil: LAT= 10^{O}S, 0^{O}, LON= 120^{O}W, 135^{O}W W-Brazil: LAT= 5^{O}S, 0^{O}, LON= 110^{O}W, 120^{O}W
STRATOZ-3 (Caravelle 116) Drummond et al., 1988	Jun 4-26, 1984	O_3	Brazil: LAT= 20^{O}S, 0^{O}, LON= 135^{O}W, 155^{O}W Canary-Islands: LAT= 20N, 35N, LON= 160^{O}W, 155^{O}W E-Tropical-N-Atlantic: LAT= 0^{O}, 20^{O}N, .LON=150W.,165W. England: LAT= 45^{O}N, 60^{O}N, LON= 10^{O}E, 5^{O}W Goose-Bay: LAT= 45^{O}N, 60^{O}N, LON= 110^{O}W, 125^{O}W Greenland: LAT= 60N, 70N, LON= 110W, 150W Iceland: LAT= 60N, 70N, LON= 150W, 155W NW-South-America: LAT=-5^{O}N, 10^{O}N, LON= 95^{O}W, 115^{O}W Puerto-Rico: LAT= 10^{O}N, 25^{O}N, LON= 110^{O}W, 120^{O}W S-South-America: LAT= 65S,45S, LON= 95W, 120W SE-South-America: LAT= 45^{O}S, 20^{O}S. LON= 115^{O}W, 140^{O}W. SW-South-America: LAT=-45^{O}S,25^{O}S, LON= 105^{O}W, 112^{O}W Spain: LAT= 35^{O}N, 45^{O}N, LON= 15W, 0^{O} W-Africa: LAT= 0., 15^{O}N, LON= 15^{O}W, 0^{O}. W-South-America: LAT= 25^{O}S, 5^{O}S. LON=

			$95^{O}W$,$110^{O}W$ Western-N-Atlantic: LAT= $25^{O}N$, $45^{O}N$, LON= $110^{O}W$,$120^{O}W$
CITE-2 (Electra) Hoell et al., 1990	Aug 11-Sep 5, 1986	O_3, NO_x, HNO_3, PAN	Calif: LAT= $35^{O}N$, $45^{O}N$, LON= $55^{O}W$, $70^{O}W$ Pacific: LAT= $30^{O}N$, $45^{O}N$, LON= $45^{O}W$, $55^{O}W$
INTEX-A,Singh et al. (2006)	Jul–Aug 2004	O3,PAN,NO_x	Eastern North America: LAT= $29^{O}N$, $51^{O}N$, Lon: $44^{O}W$-$120^{O}W$
CAIPEEX (Prabha et al., 2011)	Sep 2010 –Oct 2010	O_3, NO_x	Lat=$12^{O}N$,$22^{O}N$, Lon=$74^{O}E$, $78^{O}E$

1108

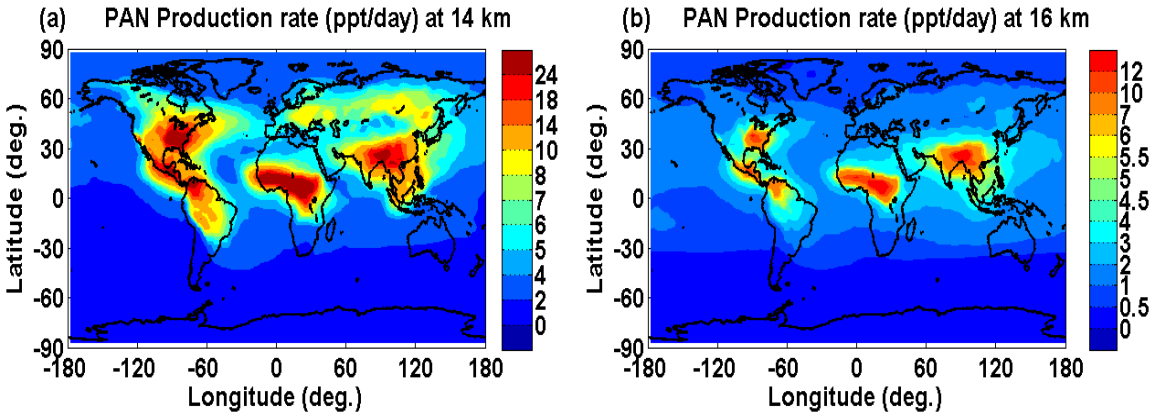

Figure 1. PAN production rates at (a) 14 km and (b) 16 km. Key regions of biomass burning and anthropogenic emissions of pollutants are evident and correspond to maxima in PAN production. Weaker dispersed background formation is evident as well.

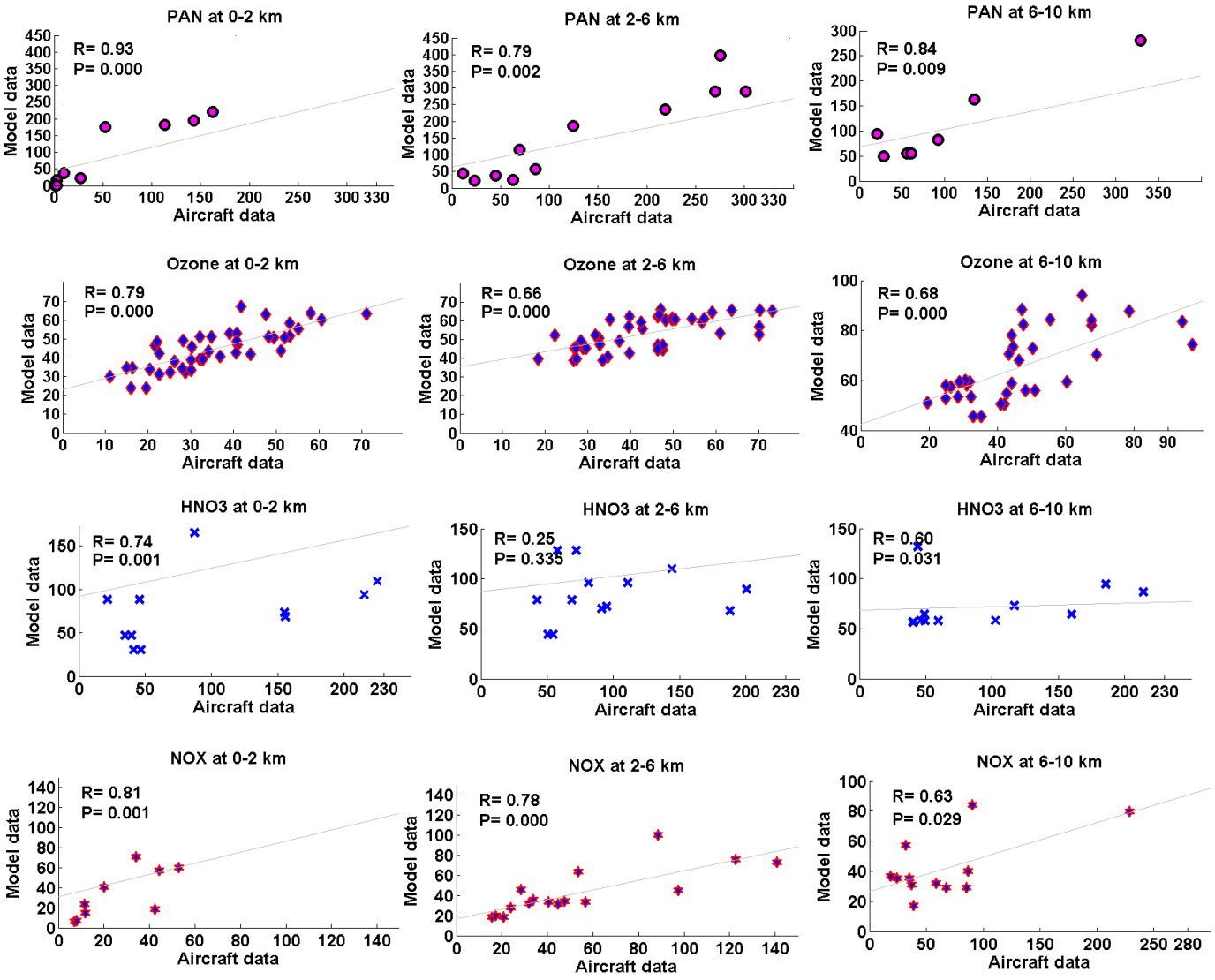

Figure 2. Scatter plot between model simulation (averaged for for 1995-2004) and aircraft observations of PAN (ppt), ozone (ppb), HNO_3 (ppt), NO_x (ppt) (averaged for the monsoon season (June-September)). The model simulations and aircraft observations are averaged for altitude ranges over the coherent regions. The Pearson's correlation coefficient (R) and corresponding p-value is given in each subplot.

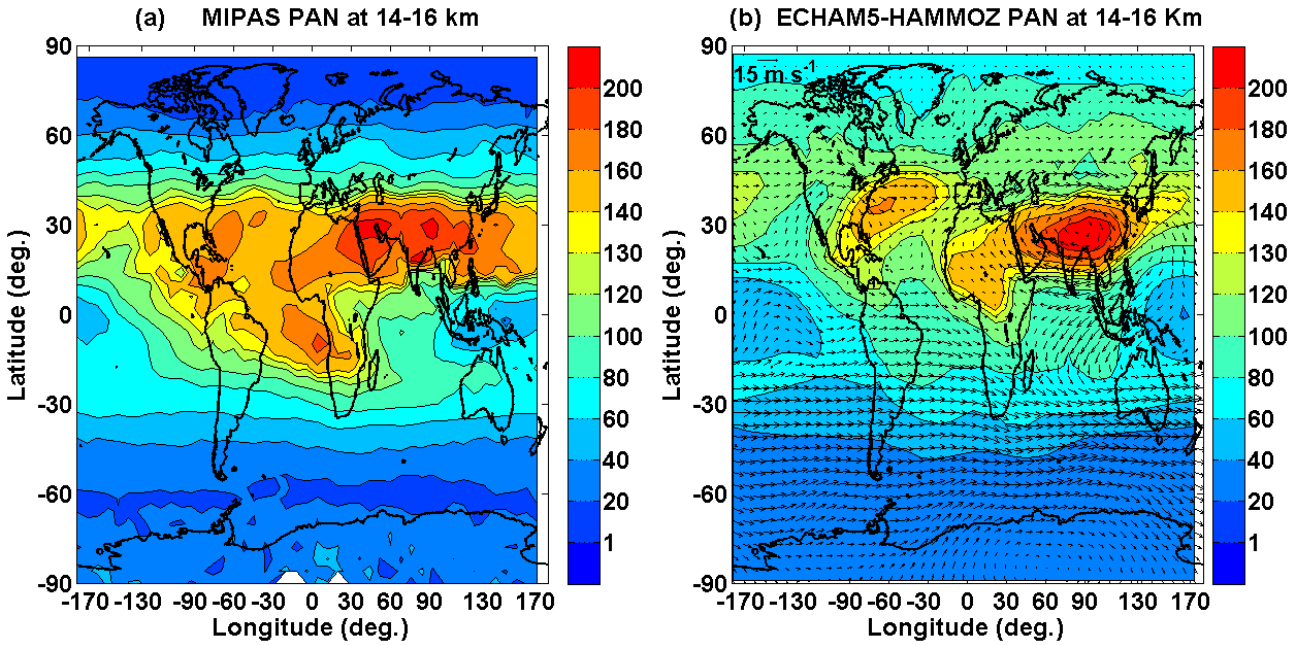

Figure 3. Distribution of seasonal mean PAN concentration (ppt) averaged for 14 -16 km (a) observed by MIPAS-E (climatology for the period 2002-2011) (b) ECHAM5-HAMMOZ CTRL simulations. Wind vectors at 16 km are indicated by black arrows in figures (b)

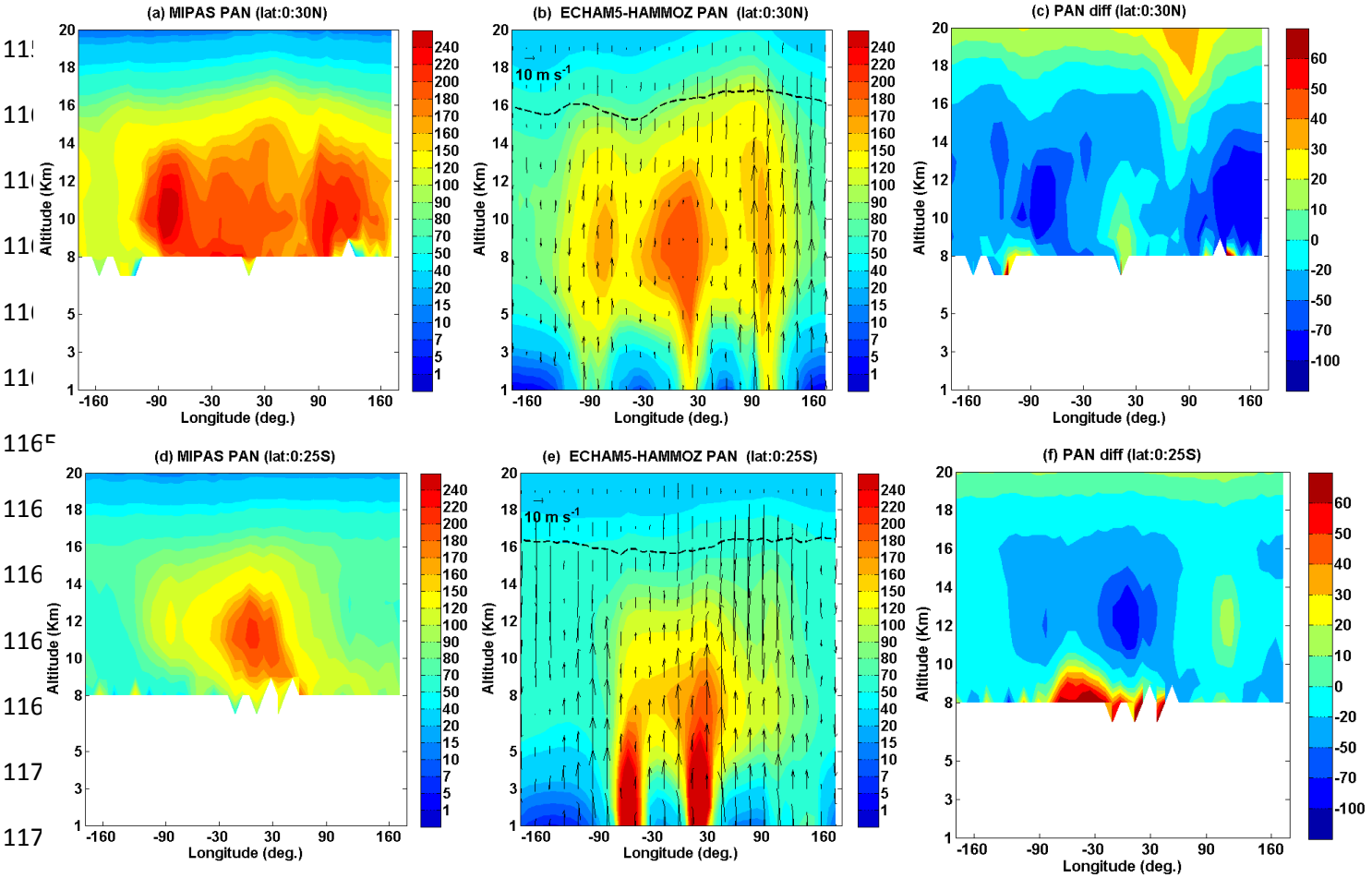

Figure 4. Longitude-altitude cross section of PAN (ppt) averaged for monsoon season and 10^{O}N - 30^{O}N; (a) MIPAS-E climatology (b) ECHAM5-HAMMOZ CTRL simulations. (c) difference in PAN (ppt) (MIPAS - ECHAM5-HAMMOZ).PAN (ppt) averaged for monsoon season and 0-25^{O}S (d) MIPAS-E climatology (e) ECHAM5-HAMMOZ CTRL simulations (f) difference in PAN (ppt) (MIPAS - ECHAM5-HAMMOZ). ECHAM5-HAMMOZ simulations are smoothed with averaging kernel of MIPAS-E. Wind vectors are indicated by black arrows in figures (b) and (e). The vertical velocity field has been scaled by 300. The black line in (b) and (e) indicates the tropopause.

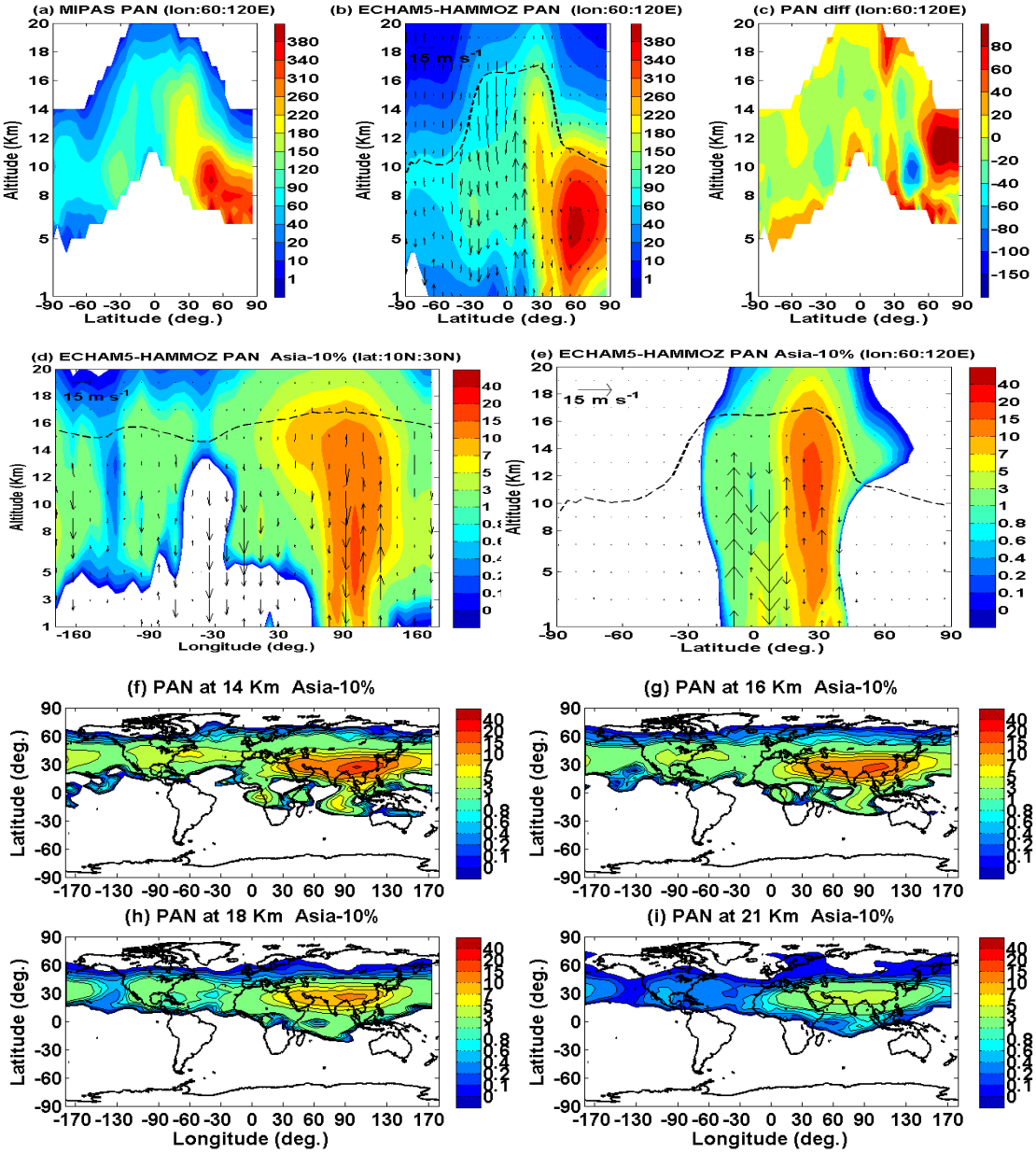

Figure 5. Latitude-altitude cross section of PAN (ppt) (a) MIPAS-E climatology, averaged for monsoon season and for 60-120^{O} E, (b) PAN from ECHAM5-HAMMOZ CTRL simulations, averaged for monsoon season and 60-120^{O} E, (c) difference in PAN (ppt) (MIPAS-ECHAM5-HAMMOZ), (d) longitude-altitude section averaged over 0 -30 ^{O} N obtained from reference-Asia-10% simulations (e) same as (d) but latitude-altitude section averaged over 60-120^{O}E, (f) – (i) latitude-longitude sections of reference – Asia-10% simulations at 14km, 16 km, 18 , 21 km respectively. Wind vectors are indicated by black arrows. The vertical velocity field has been scaled by 300.

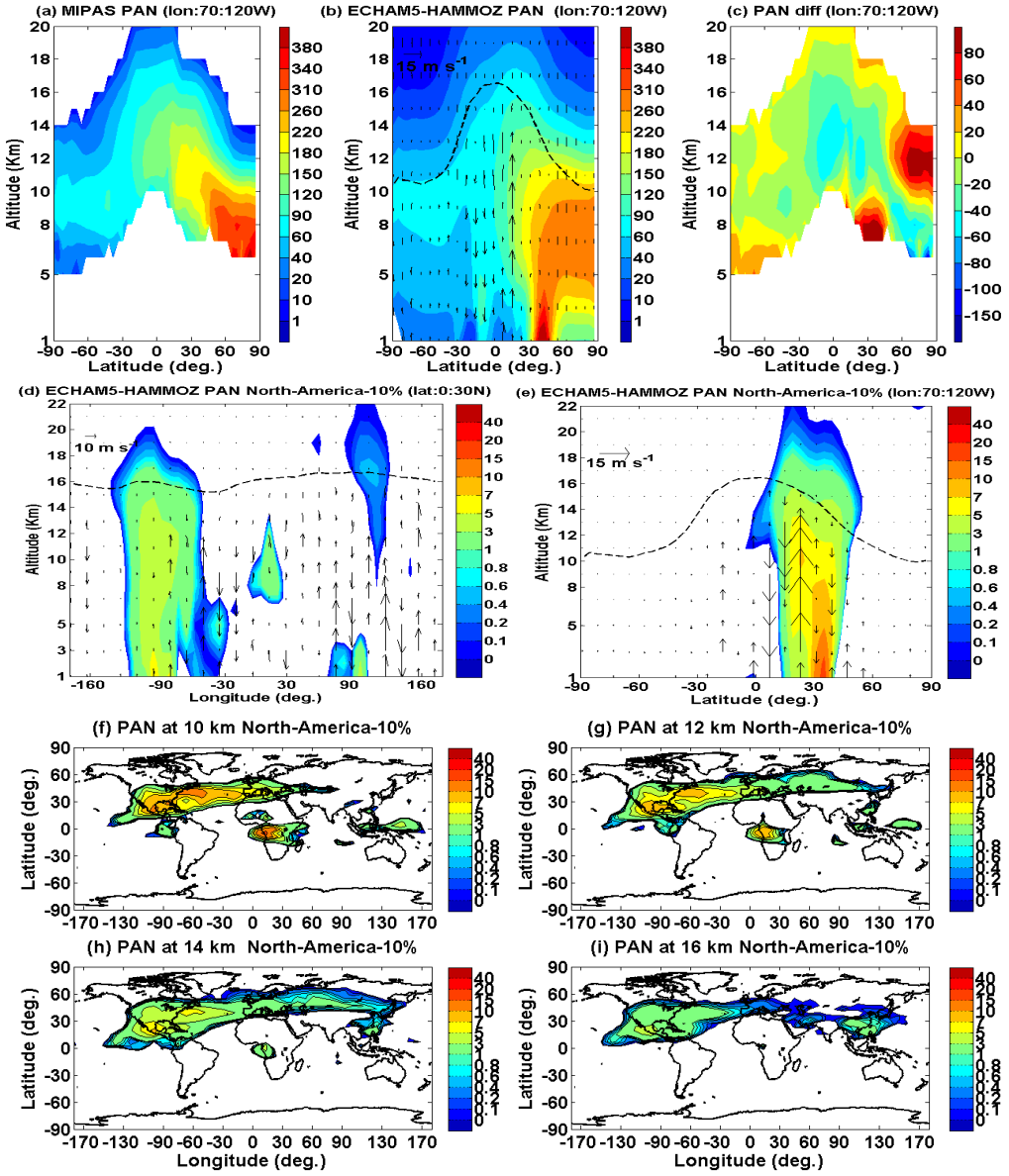

Figure 6. Latitude-altitude cross section of PAN (ppt) (a) MIPAS-E climatology, averaged for monsoon season and for 70-120^{O} W, (b) PAN from ECHAM5-HAMMOZ CTRL simulations, averaged for monsoon season and 70-120^{O} E, (c) difference in PAN (ppt) (MIPAS-ECHAM5-HAMMOZ), (d) longitude-altitude section averaged over 0 -30 ^{O} N obtained from reference-North-America-10% simulations (e) same as (d) but latitude-altitude section averaged over 120^{O}W-70^{O}W, (f) –(i) latitude-longitude sections of reference – North-America-10% simulations at 10km, 12 km 14km, 16 km respectively. Wind vectors are indicated by black arrows. The vertical velocity field has been scaled by 300.

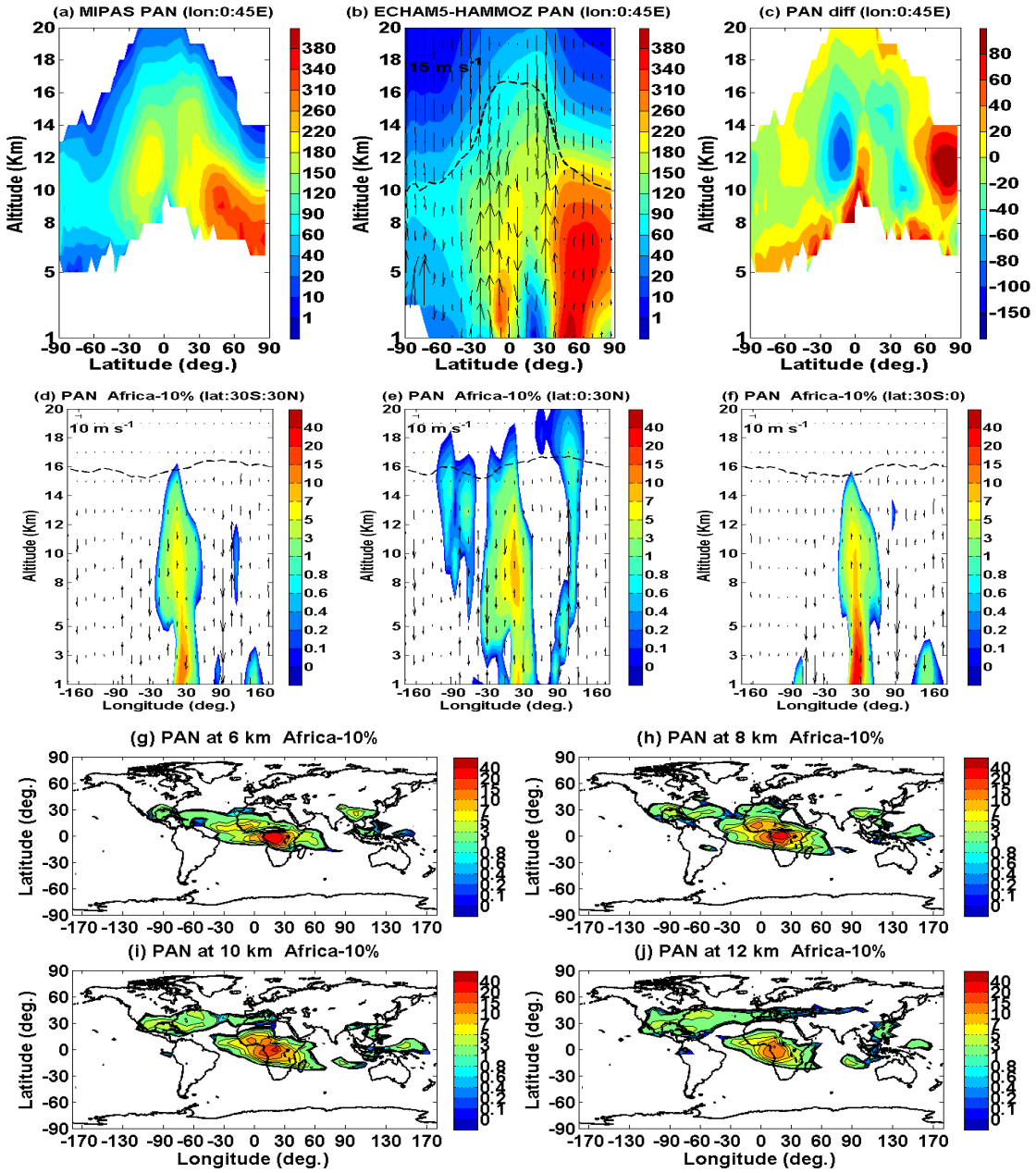

Figure 7. Latitude-altitude cross section of PAN (ppt) (a) MIPAS-E climatology, averaged for monsoon season and for 0-45^{O} E, (b) PAN from ECHAM5-HAMMOZ CTRL simulations, averaged for monsoon season and 0-45^{O} E, (c) difference in PAN (ppt) (MIPAS-ECHAM5-HAMMOZ), (d) longitude-altitude section averaged over 30 ^{O}S - 30 ^{O}N obtained from reference-Africa-10% simulations (e) same as d but averaged over 0-30^{O}N, (f) same as d but averaged over 0-30^{O}S.Wind vectors are indicated by black arrows. The vertical velocity field has been scaled by 300, Longitude – latitude section of PAN obtained from reference- Africa-10% simulations at (g) 6 km, (h) 8 km, (i) 10 km, (j) 12km.

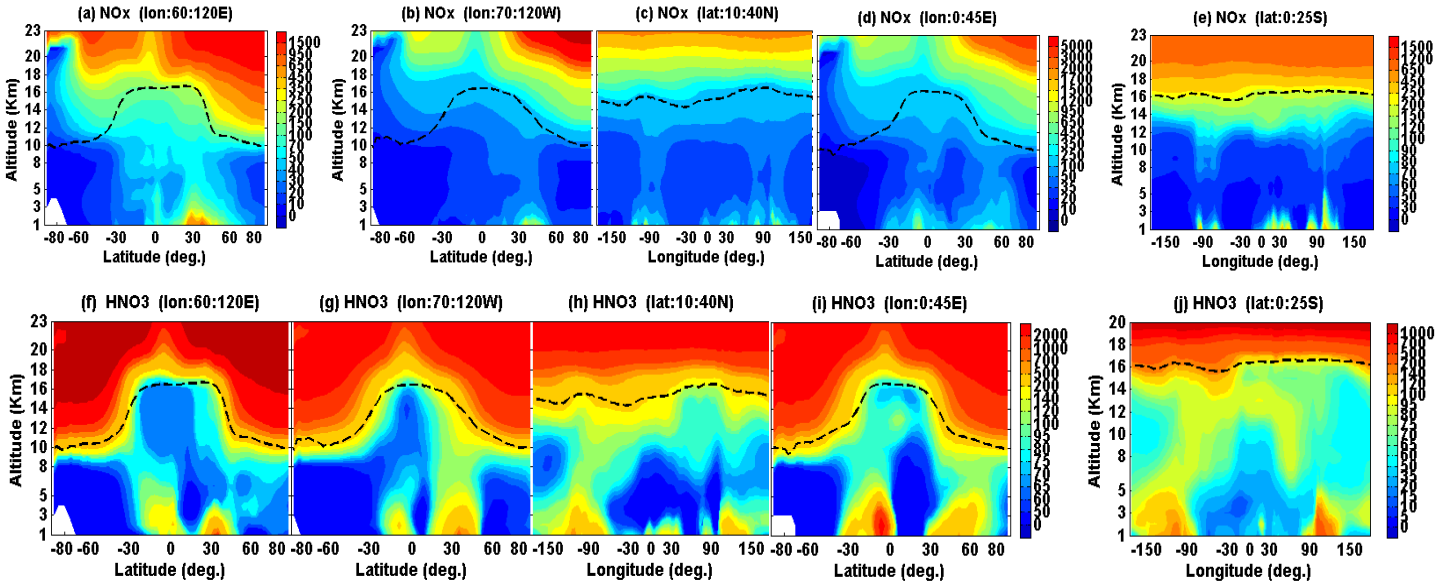

Figure 8. Panel (a) Latitude-altitude cross section of seasonal mean ECHAM5-HAMMOZ NO_x (ppt) averaged for (a) 60^O E-120^O E, (b) 70^O W-120^O W, (c) longitude-altitude cross section averaged over 10^O N-40^O N, (d) latitude-altitude cross section averaged over 0-45^O E and (e) longitude-altitude cross section averaged over 0-25^O S, (f)-(i) same as (a)-(e) but for HNO_3.

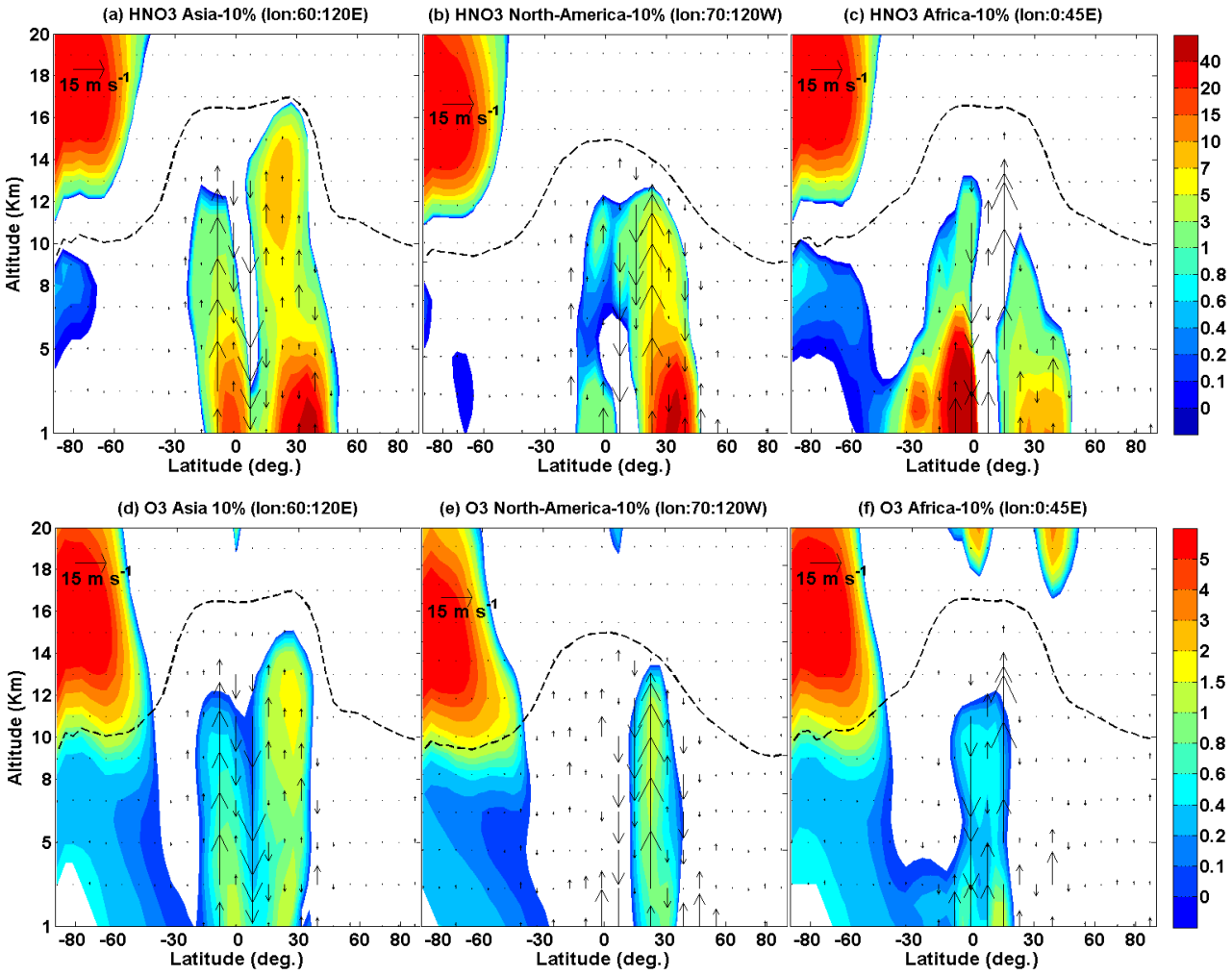

Figure 9. Latitude-altitude variation of (a) HNO_3 (Reference – Asia-10%) , averaged over 60^{O}-120^{O}E (b) HNO_3 (difference of Reference – North-America-10%) , averaged over 70^{O}-120^{O}W (c) HNO_3 (Reference – Africa-10%), averaged over 0-45^{O} E (d) O_3 (difference of Reference – Asia-10%) averaged over 60-120E (e) O_3 (Reference – North-America-10%) over North America averaged over 70^{O} -120^{O} W (f) O_3 (Reference – Africa-10%) over Africa averaged over 0-45(Reference – Africa-10%) . HNO_3 is expressed in ppt and ozone in ppb.

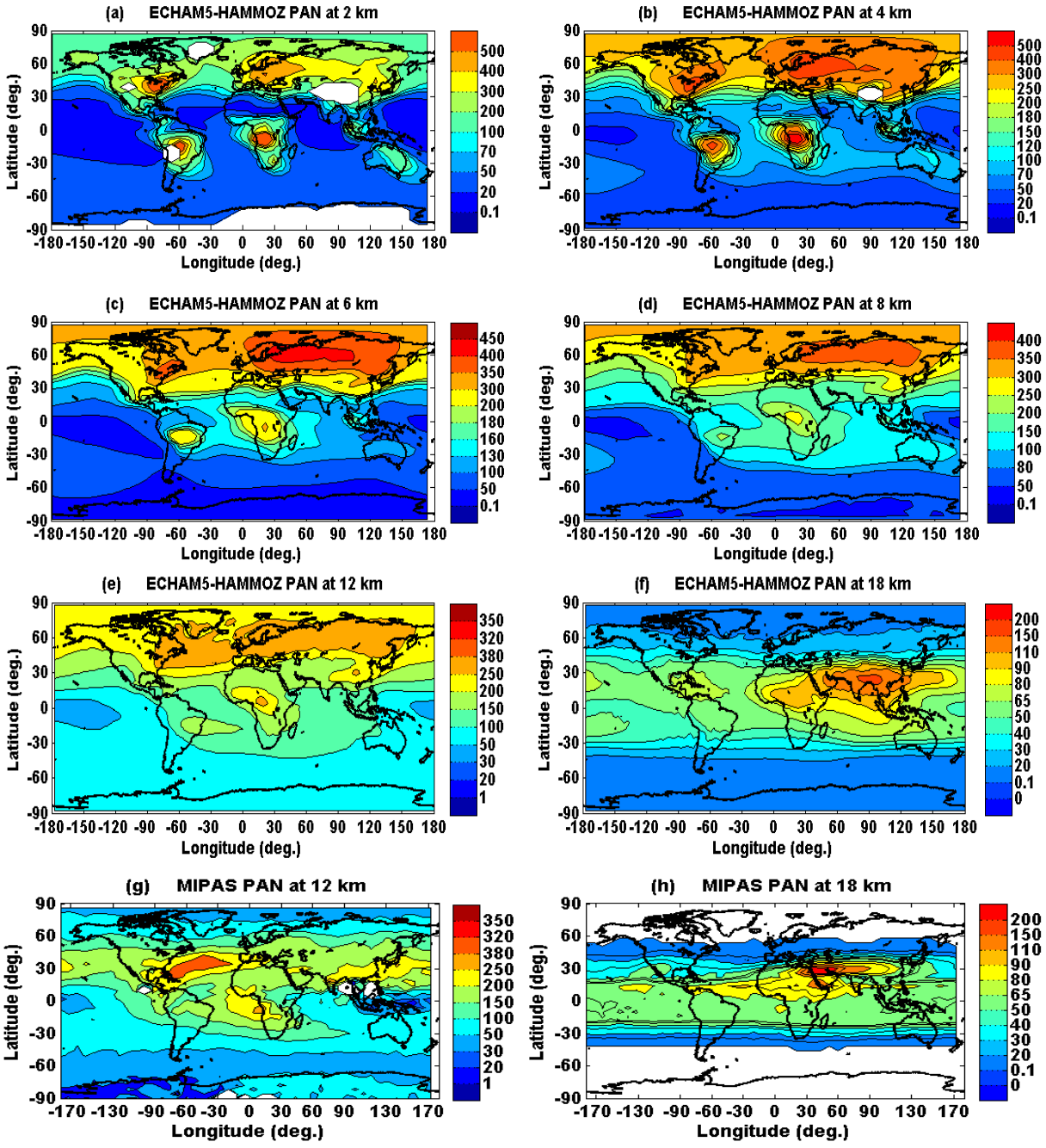

Figure 10. Latitude-longitude cross section of PAN (ppt) averaged for monsoon season (a) ECHAM5-HAMMOZ simulations at 2 km (b) 4 km (c) 6 km (d) 8 km (e) 12 km (f) 18 km. MIPAS-E climatology at (g) 12 km (h) 18 km.

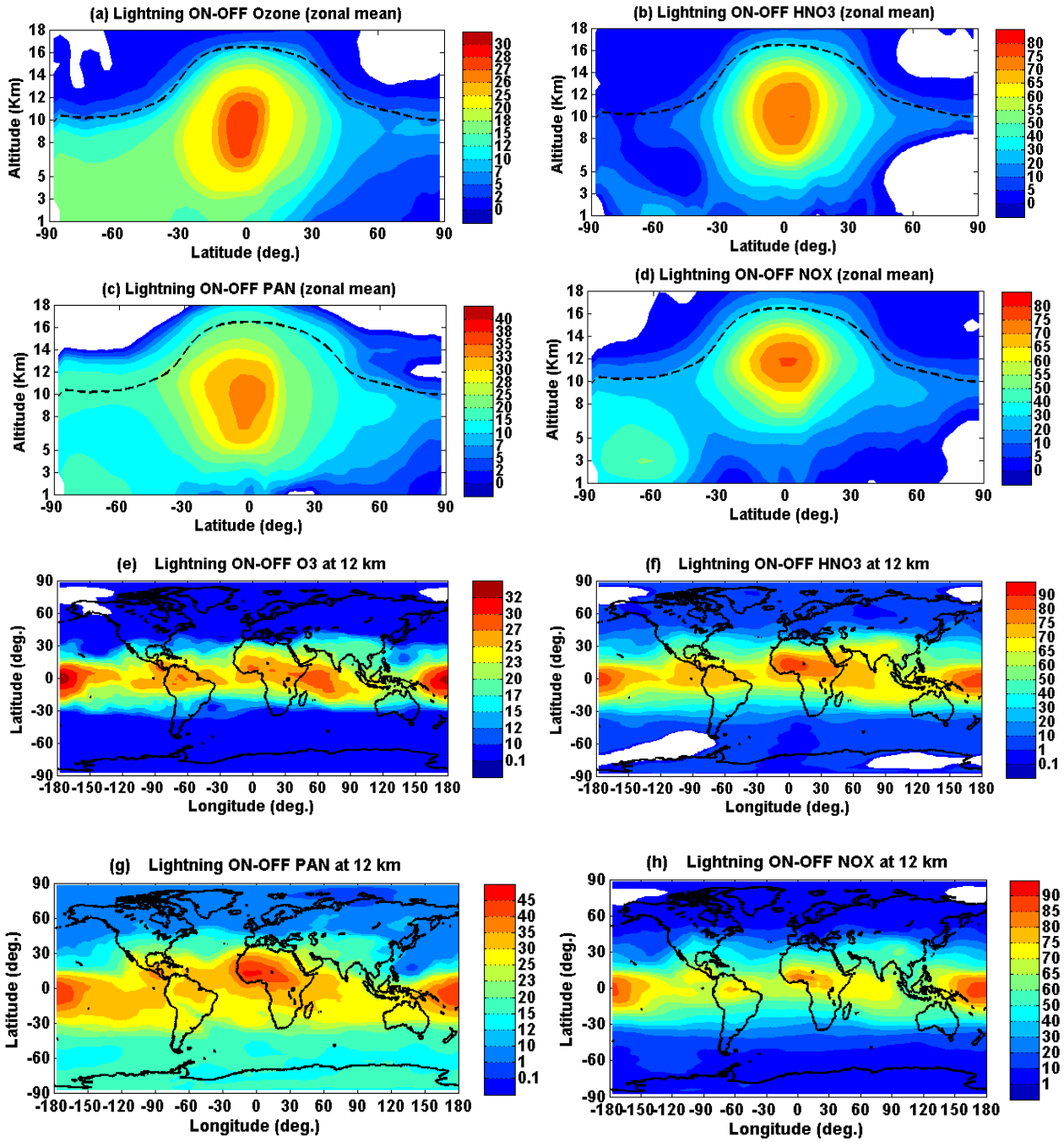

Figure 11. Zonal averaged seasonal mean changes (percentage) produced from lightning in (a) ozone (b) HNO_3 (c) PAN (d) NO_x, distribution of seasonal mean changes (percentage) produced from lightning in (e) ozone (f) HNO_3 (g) PAN (h) NO_x at 12 km.